Journal of Controlled Release 377 (2025) 17–36

Contents lists available at ScienceDirect

Journal of Controlled Release

journal homepage: www.elsevier.com/locate/jconrel

# Bioinspired orthogonal-shaped protein–biometal nanocrystals enable oral protein absorption

Matilde Durán-Lobato [a,b,c,d], Sulay Tovar [a,b,e], Juan Cuñarro [a,b], Rocío Ramos-Membrive [f,g], Iván Peñuelas [f,g], Ilaria Marigo [h,i], Federico Benetti [j], Miguel Chenlo [k], Clara V. Álvarez [k], Vashegyi Ildikó [l], Rudolf Urbanics [l,m], János Szebeni [n,o,p], María José Alonso [a,b,c,*]

[a] Center for Research in Molecular Medicine & Chronic Diseases (CIMUS), University of Santiago de Compostela, Campus Vida, 15782 Santiago de Compostela, Spain
[b] Health Research Institute of Santiago de Compostela (IDIS), University of Santiago de Compostela, Campus Vida, 15782 Santiago de Compostela, Spain
[c] Department of Pharmacology, Pharmaceutics and Pharmaceutical Technology, School of Pharmacy, University of Santiago de Compostela, 15782 Santiago de Compostela, Spain
[d] Departamento de Farmacia y Tecnología Farmacéutica, Facultad de Farmacia, Universidad de Sevilla, Prof. García González, 2, 41012 Seville, Spain
[e] CIBER Fisiopatología de la Obesidad y Nutrición (CIBERobn), Madrid, Spain
[f] Radiopharmacy Unit, Department of Nuclear Medicine, Clínica Universidad de Navarra, Instituto de Investigación Sanitaria de Navarra (IdiSNA), Av. Pío XII 36, 31008 Pamplona, Spain
[g] Translational Molecular Imaging Unit, Department of Nuclear Medicine, Clínica Universidad de Navarra, Instituto de Investigación Sanitaria de Navarra (IdiSNA), Av. Pío XII 36, 31008 Pamplona, Spain
[h] Department of Surgery, Oncology and Gastroenterology, University of Padova, Padova, Italy
[i] Veneto Institute of Oncology IOV-IRCCS, Padova, Italy
[j] ECSIN-European Center for the Sustainable Impact of Nanotechnology, ECAMRICERT SRL, Padova, Italy
[k] Neoplasia & Endocrine Differentiation P0L5, Centre for research in Molecular Medicine and Chronic Disease (CIMUS), Av Barcelona s/n, 15782 Santiago de Compostela, Spain
[l] SeroScience Ltd, Budapest, Hungary
[m] Nanomedicine Research and Education Center, Department of Pathophysiology, Semmelweis University, Budapest, Hungary
[n] Nanomedicine Research and Education Center, Department of Translational Medicine, Semmelweis University, Budapest 1089, Hungary
[o] Department of Nanobiotechnology and Regenerative Medicine, Faculty of Health Sciences, Miskolc University, Miskolc 2880, Hungary
[p] School of Chemical Engineering and Translational Nanobioscience Research Center, Sungkyunkwan University, Suwon 16419, Republic of Korea

ARTICLE INFO

*Keywords:*
Peptide delivery
Protein delivery
Oral delivery
Transmucosal
Biologicals
Nanocomplexes

ABSTRACT

With the growing number of marketed biological drugs, the development of technological strategies for their oral systemic absorption, becomes increasingly important. The harsh gastrointestinal environment and low permeability of the intestinal epithelium, represent a huge challenge for their systemic delivery. Herein, bioinspired in the physiological insulin-Zn interaction, the design of orthogonal-shaped protein-biometal hybrid nanocrystals, further enveloped by a bilayer of functional biomaterials, is reported. The nanocrystals exhibited a size of 80 nm, a neutral surface charge and a high insulin loading. In vitro studies showed the capacity of the nanocomplexes to control the release of the associated insulin, while preserving its stability. In vivo evaluation showed sustained blood glucose reductions in both healthy and diabetic rats (up to 40 % and 80 %, respectively), while chronic immunotoxicity studies in mice indicated no toxicity effect. Preliminary efficacy studies in healthy awake pigs following oral capsule administration showed over 20 % absolute bioavailability.

## 1. Introduction

Protein/peptide therapeutics have a prominent role in current and future healthcare market scenarios, mainly because their macromolecular structures make them more specific and potent than small molecules [1]. However, their structural complexity makes them vulnerable in physiological environments and inefficient at overcoming biological barriers to systemic delivery [1,2]. As a result, peptide

* Corresponding author at: Center for Research in Molecular Medicine & Chronic Diseases (CIMUS), University of Santiago de Compostela, Campus Vida, 15782 Santiago de Compostela, Spain.
*E-mail address:* mariaj.alonso@usc.es (M.J. Alonso).

https://doi.org/10.1016/j.jconrel.2024.11.016
Received 30 March 2024; Received in revised form 13 October 2024; Accepted 7 November 2024
Available online 17 November 2024

therapeutics are currently administered mainly via injection [3]. which limits their use in chronic treatments.

The oral route is by far the most useful and acceptable modality of drug administration [4]. Consequently, significant efforts have been devoted to overcoming each of the major barriers identified for oral protein delivery, namely, the harsh gastrointestinal environment, the mucus layer and the underlying epithelial barrier [5]. The strategies developed thus far include the use of protease inhibitors and/or permeation enhancers, the chemical modification of peptides for tuning their physicochemical profiles [6], and a wide range of polymeric-, lipid- and complex-based nanocarriers [3,7]. Furthermore, technologies previously applied in other fields have been explored for oral-route applications, such as ionic liquids [8] and iontophoresis [9], while complex microneedle capsule designs have emerged [10–14]. Nevertheless, success has been elusive thus far; there has been extensive preclinical research but currently very few technologies in early clinical evaluation [5,7], and only two formulations, based on permeation enhancers, have been recently approved for commercialization [15,16].

The ultimate remaining obstacle is low oral bioavailability along with high intra- and intersubject response variability [7]. On the other hand, translational aspects, such as biomaterial quality and safety, robust design performance, conversion into a final solid dosage form, production technology scalability and cost/benefit balance frequently remain underrated, hampering clinical translation [7,17].

In order to overcome both biological and technological barriers, this work focused on designing a new generation of oral protein nanomedicines inspired by physiological phenomena. Specifically, our inspiration derived from the observation of natural insulin-Zn complexes in the pancreatic storage deposits [18]. This extensively studied protein–biometal interaction [19,20] has been widely exploited for prolonging insulin release following parenteral administration, leading to the co-addition of Zn salts to encapsulate insulin in micro- and nanocarriers [21–24], where an excess of Zn decreased the solubility of insulin [24]. However, the potential of such an interaction has never been exploited as a nanocarrier in itself, and more specifically for the formation of ultrasmall (below 100 nm), orthogonally shaped insulin-Zn nanocrystals, and their use for oral insulin delivery. Hence, herein, we report a potential nanomedicine candidate consisting of tunable insulin-Zn orthogonal nanocomplexes endowed with the capacity to overcome the biological barriers associated with the oral route. To enhance their stability and promote interaction with enterocytes, the nanocrystals were coated with a bilayer of amphiphilic materials, specifically lauroyl arginate ester (LAE) and polyethylene glycol stearate (PEGst). This bilayer was designed to mimic the phospholipid architecture of a cell membrane while exposing a neutral hydrophilic surface.

The nanocarriers were evaluated in terms of their key physicochemical properties and colloidal stability, controlled release and protection against enzymatic degradation in biologically relevant media. Additionally, the freeze-dried form of the nanocarriers was evaluated to assess the preservation of nanocarrier properties and the bioactivity of the processed protein. Furthermore, in vivo efficacy studies were conducted in both healthy and diabetic rat models and a 28-day chronic immunotoxicity study in mice was performed. In a final step, an enteric capsule dosage form containing the freeze-dried powder of the formulation was administered to healthy awake pigs and the insulin bioavailability was determined.

## 2. Results and discussion

### 2.1. Rational design and production of enveloped insulin-Zn nanocomplexes

The design was based on the hypothesis that the new nanoformulation would protect insulin from intestinal enzymes, navigate through the mucus layer and facilitate the interaction with the underlying epithelium. The key quality attributes of a targeted insulin nanocarrier include a reproduceable non-spherical nanoscale size, high protein association and loading, sustained release, colloidal stability in intestinal fluids, mucodiffusive character and the ability to promote the interaction with the epithelium. Additionally, the technological requisites include biomaterial safety, production scalability and reproducibility, and the generation of a final solid dosage form suitable for oral administration.

Given the required insulin dose and the dilution in the orally administered dried form, significant attention was focused on achieving a high insulin loading (quantity of insulin/quantity of nanocarrier). To this aim, our bioinspiration relied on the insulin-Zn complex naturally occurring in the pancreas and involved in physiological insulin metabolism [25]. This interaction has served as the basis for some sustained-release formulations already on the market [21,23,26], and Zn salts and insulin mixtures have been widely employed as encapsulated materials in micro- and nanocarriers [21–23] for protein aggregation, thus favoring insulin encapsulation and delaying its release. However, the technological approach adopted here is radically different. Indeed, the aim was to design and develop hybrid orthogonal-shaped insulin-Zn nanocrystals stabilized by a bilayer of functional biomaterials with penetration enhancing properties. Such configuration was achieved in a first stage by adopting a bottom-up methodology, that allowed to produce structured insulin-Zn nanocomplexes with tunable physicochemical properties controlled by selected process conditions. We identified the following parameters as critical for achieving optimal nanosystem properties: i) the optimal insulin:Zn molar ratio was 1:6, ensuring the complete hexameric complexation of the protein and maximized association (Fig. 1A); ii) the optimal incubation media pH was 5.1, resulting in a low particle size (<100 nm) and polydispersion index (PDI) of <0.3 (Fig. 1B, C, Table S1), which was attributed to optimized protein ionization and subsequent interaction with Zn cations; and iii) stabilization of the complexation step at 4 °C, leading to a reduced particle size and more homogenous system crystallization (Table S2). The nanocomplexes presented an ~80 nm size, a 0.3 PDI and a negative zeta potential (ZP) (Fig. 1E). Their small size was expected to favor intestinal cell interactions and mucodiffusion [27], and the negatively charged surface was attributed to negatively charged insulin residues at the final pH of 6.8 of the nanocomplex suspension media [28]. This is consistent with the hexameric structure of the insulin-Zn complex, where Zn ions are found in an inner axial position coordinated with histidine side chains [29]. A remarkable association efficiency of close to ~100 % with a final loading of over 90 % was obtained (Fig. 1E). Such exceptional drug loading is crucial for achieving the required oral dose after final packaging into oral solid dosage forms.

Transmission electron microscopy (TEM) imaging (Fig. 1F) interestingly revealed a population of non-spherical polygonal nanostructures with a significantly smaller size of approximately 50 nm and lower polydispersion compared to dynamic light scattering (DLS) analysis. The orthogonal shape of the structures was attributed to the crystal nature of the pure insulin-Zn complex [30]. This shape was considered to be the cause of the overestimation of the particle size and polydispersity values obtained by DLS analysis, as this technique is adapted to spherical particles [31]. Nanoparticle geometry has been recently identified as a parameter with substantial impact on oral uptake and transport [32], influencing the retention time in the gastrointestinal tract [33], mucus permeation, cellular uptake, intracellular processing and transmembrane transport [33–35]. Overall, the improved performance of non-spherical particles has been attributed to their larger contact surface area [32], and modified Brownian movement, rotation around the mucus networks and shear flow [34,36].

### 2.2. Surface envelopment of the nanocomplexes with a cosurfactant bilayer

Next, the nanocomplexes were enveloped by a hydrophilic neutral surfactant bilayer to provide colloidal stability, improved mucodiffusion

A

| Insulin:Zn molar ratio | Incubation pH | Final pH | Size (nm) | PDI | Loading efficiency (%) |
|---|---|---|---|---|---|
| 1:3 | 5.5 ± 0.0 | 7.3 ± 0.0 | 123.7 ± 28.3 | 0.4 | 68.1 ± 2.8 |
| 1:6 | 5.4 ± 0.1 | 7.0 ± 0.1 | 121.2 ± 10.3 | 0.3 | 91.7 ± 2.9 |
| 1:10 | 5.3 ± 0.1 | 6.8 ± 0.1 | 120.8 ± 3.7 | 0.2 | 84.3 ± 1.2 |

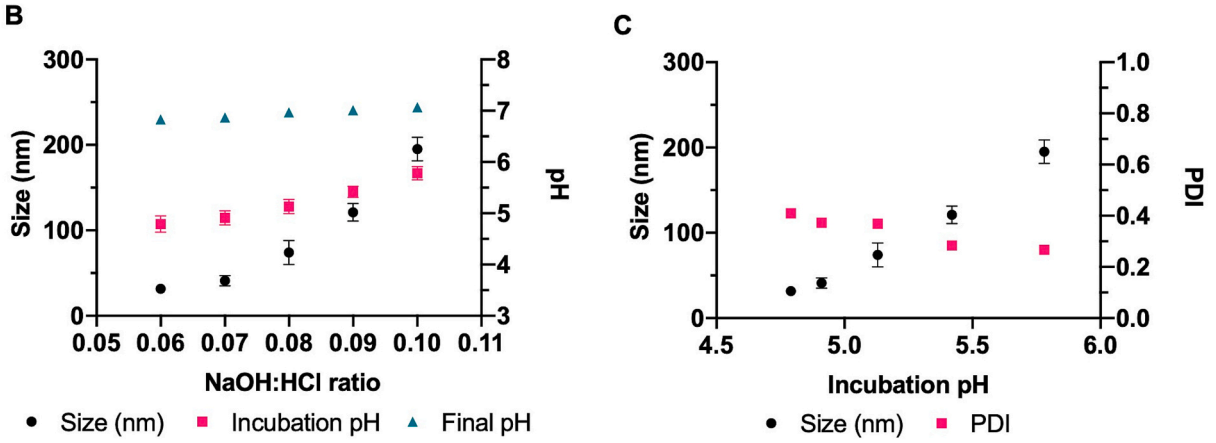


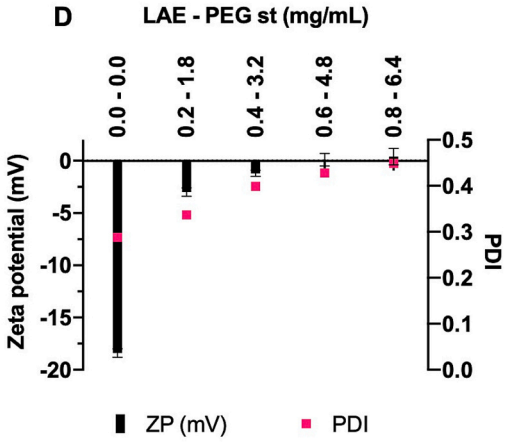


E

| Coating | Batch Size (mL) | Size (nm) | PDI | ZP (mV) | Initial loading (%) | Loading efficiency (%) |
|---|---|---|---|---|---|---|
| None | 2 | 76 ± 15 | 0.3 | -15 ± 3 | 92.6 | 91.2 ± 3.7 |
| Yes | 2 | 83 ± 7 | 0.4 | 0.4 ± 0.8 | 10.0 | 95.2 ± 5.3 |
| Yes | 20 | 85 ± 11 | 0.4 | -1.0 ± 1.1 | 10.0 | 94.1 ± 1.9 |
| Yes | 200 | 79 ± 5.6 | 0.4 | 0.3 ± 0.7 | 10.0 | 91.7 ± 2.9 |

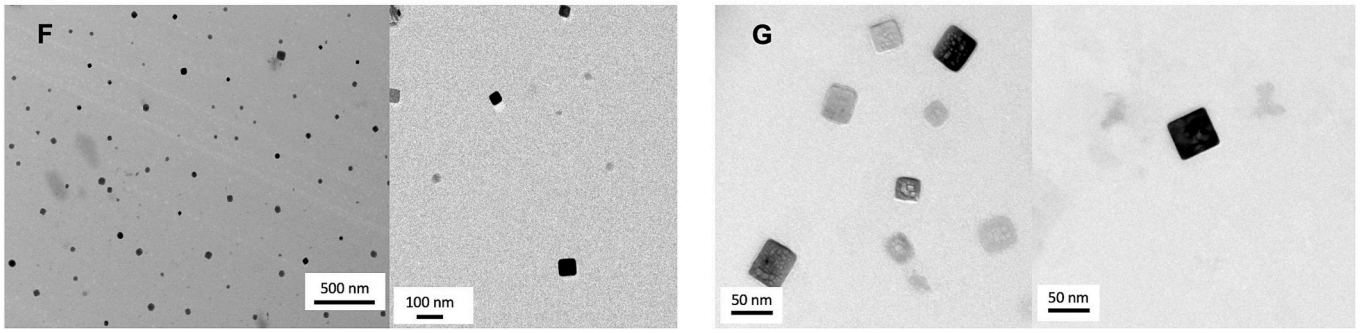


**Fig. 1.** Bottom-up production of enveloped nanocomplexes. A, pH values adjusted during the production process and resulting physicochemical parameters of the formulations as a function of the employed insulin:Zn ratio. Several ratios [37] were assayed to ensure maximized protein hexameric complexation, and a ratio of 1:6 was finally selected as optimal (over 90 % association). B, pH values in the production process, particle size and PDI measured by DLS of screened formulations as a function of the employed acid-base volume ratios (NaOH 0.1 N: HCl 0.01 N). C, Graphic representation of the particle size and PDI of the formulations as a function of pH at the incubation step. A pH value of 5.1 (NaOH:HCl volume ratio 0.08) was selected for further development, since it allowed us to maintain a small particle size (<100 nm) along with an acceptable PDI value (0.3). D, ZP and PDI values of the nanocomplexes upon addition of increasing concentrations of LAE-PEGst coating, leading to neutral ZP values and increased PDI. E, Physicochemical parameters of formulations before and after coating and upon increasing batch size (10- and 100-fold) after adapting the production process, validating the scaling-up trial. F, TEM images of plain nanocomplexes. G, TEM images of enveloped nanocomplexes. All measurements and error bars are displayed as the mean values ± SDs ($n = 3$).

[38], protection against enzymatic degradation [39] and enhanced epithelial penetration [40]. For this purpose, a combination of neutral and positively charged amphiphilic molecules was selected, specifically PEGst, a widely employed FDA-approved excipient, and LAE, an arginine-based biologically derived generally-regarded-as-safe (GRAS) excipient [41]. Both molecules were expected to act synergistically based on their reported capacity to interact with cell membranes and alter their permeability [42]. Briefly, PEGst and LAE were sequentially added to a nanocomplex suspension at an 8:1 PEGst:LAE mass ratio, since a higher relative amount of LAE compared to PEGst (lower PEGst: LAE mass ratio) led to nanocomplex aggregation. By increasing the amount of both PEGst and LAE added to the formulation, while maintaining the optimized PEGst:LAE mass ratio, the ZP of the formulation increased to neutral values (Fig. 1D) while the mean particle size was maintained, thus indicating the surfactant interaction with the nanosystem surface. Interestingly, the PDI values increased, particularly when the ZP values attained neutrality (Fig. 1D), due to an excess of surfactant molecules forming micelles. TEM imaging confirmed that the nanocomplex size and morphology remained unaltered after the enveloping step (Fig. 1G). A concentration of 0.8 mg/mL LAE–6.4 mg/mL PEGst in the final nanocomplex suspension was selected on account of the resulting neutral ZP, indicating the complete coverage of the nanocomplex surface. The resulting formulation was successfully freeze-dried (Fig. S1 and S2).

### 2.3. Architectural organization of the orthogonal crystalline nanocomplexes enveloped by a surfactant bilayer

Freeze-dried samples of the enveloped nanocomplexes were analyzed by X-ray diffraction (XRD), where the widening of the highest intensity peaks in a diffractogram is related to the size of the crystalline domains. Overall, wide peaks or bands attributable to nanocrystalline domains were identified for both trehalose and PVP-mannitol formulation powders (Fig. 2B, C), while control samples presented either no peaks or narrow peaks indicative of nonnanocrystalline domains, altogether suggesting the presence of nanocrystallites in the formulation.

The cosurfactant envelope architecture, initially understood as depicted in Fig. 3A based on experimental results, was further investigated. For instance, when only LAE was added to the nanocrystal suspension, the nanoparticles immediately aggregated due to the interaction of positively charged LAE molecules with the negatively charged nanocomplexes. On the other hand, when only PEGst was added to the nanocomplexes, no change in the physicochemical properties of the nanocomplexes was observed. However, when PEGst and LAE were

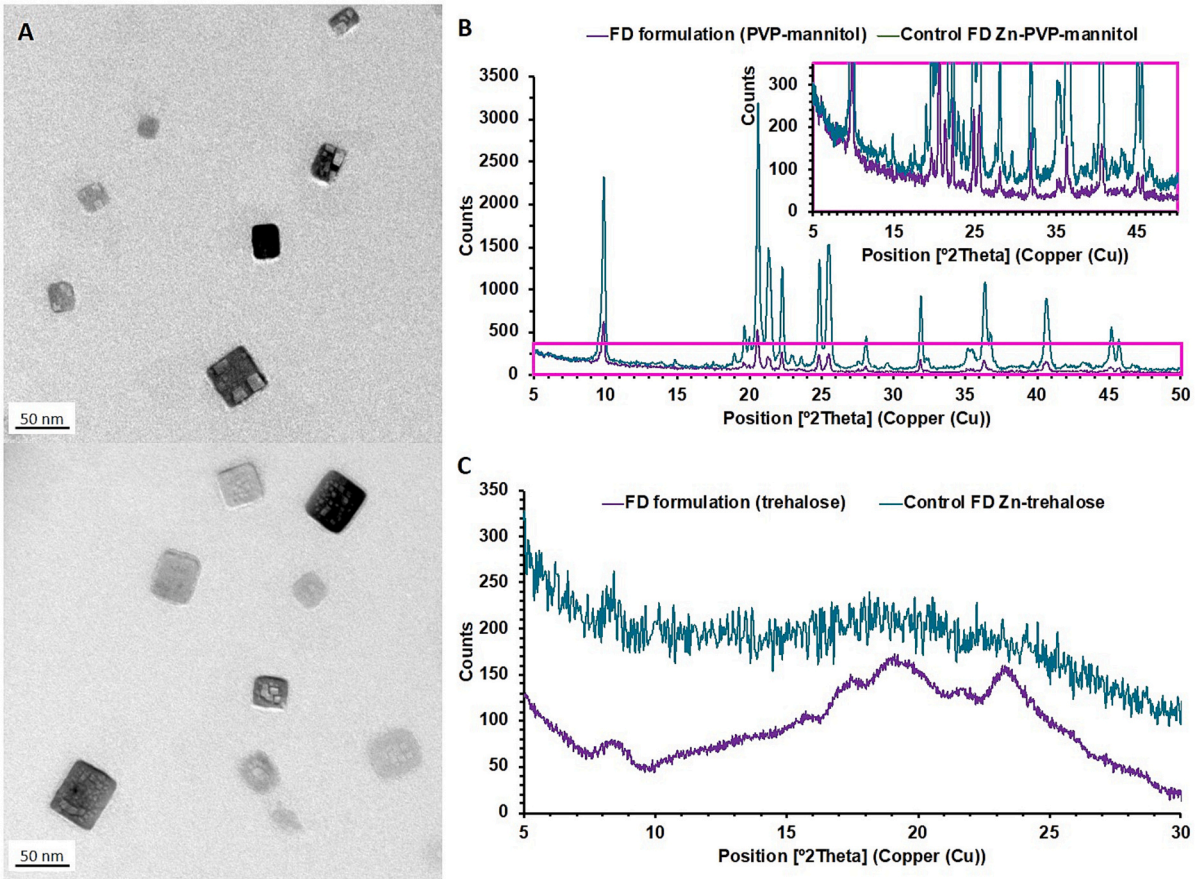


**Fig. 2.** Characterization of the inner crystalline nanocomplex structure. X-ray analysis was performed to assess whether the nanocomplexes presented the known crystalline structure [30] of the insulin-Zn hexameric complex. A, TEM imaging of nanocomplexes showing inner structural patterns. B, X-ray diffractogram of nanocomplexes freeze-dried with PVP-mannitol (purple line) and control sample of the freeze-dried solution of PVP-mannitol and zinc (green line) at the same concentrations as in the formulations. The diffractogram of the nanocomplexes (purple line) presented several narrow peaks coincident with those of the zinc control sample (green line), which indicated the nonnanocrystalline domains attributed to mannitol. However, the formulation powder also presented wider peaks attributable to nanocrystalline domains, which were not present in the zinc control sample diffractogram, where higher narrower peaks appeared instead (14 to 18°2Th and 23 to 24°2Th). C, X-ray diffractogram of nanocomplexes freeze-dried with trehalose (purple) and control samples of freeze-dried trehalose and zinc (green line). The absence of crystalline phases for the control trehalose-zinc sample (green line) allowed more accurate identification of crystalline domains for the freeze-dried formulation (purple line). The diffractogram of nanocomplexes freeze-dried with trehalose (purple line) presented several wide peaks or bands indicative of nanocrystalline domains, attributed to the nanocomplex core structure. (For interpretation of the references to colour in this figure legend, the reader is referred to the web version of this article.)

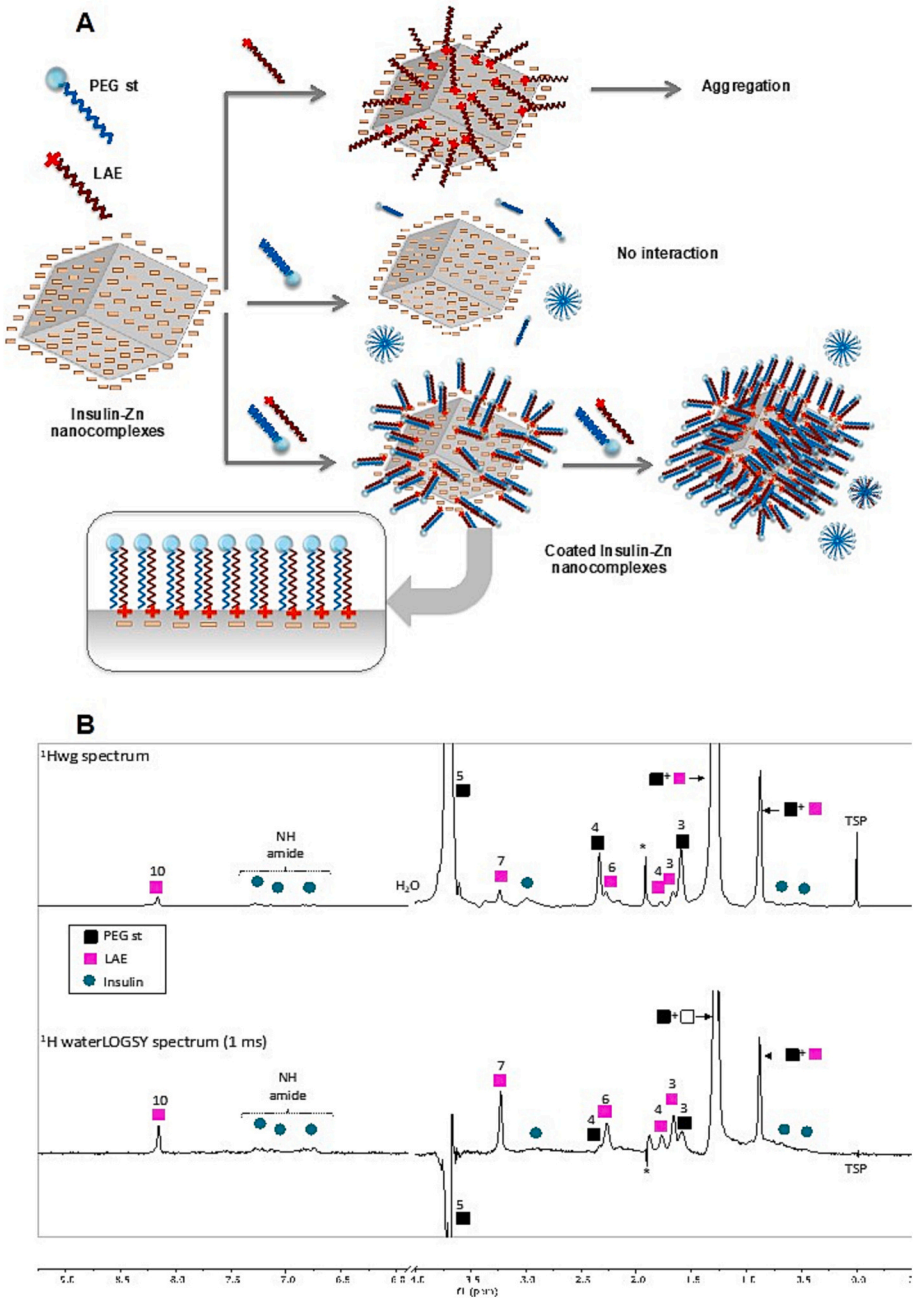


**Fig. 3.** Characterization of the surfactant bilayer envelope. A, Schematic picture showing the hypothesized conformation of the bilayer of amphiphilic biomaterials based on experimental results. B, $^{1}$H NMR and waterLOGSY (water-ligand observed via gradient spectroscopy) analysis of the enveloped nanocomplexes. Detailed $^{1}$H NMR signal assignment and diffusion-ordered spectroscopy (DOSY) experiments disregarding the influence of surfactant molecules not attached to the nanocomplex surface are available in the SI section. The waterLOGSY spectrum clearly showed a 3.71 ppm inverted peak corresponding to PEG regions, while the signal corresponding to bulk aliphatic chains from both surfactants (1.27 ppm) remained noninverted. The observed changes in the signals were proportional to the length of the applied pulse (from 3 to 1 ms, SI section), thus confirming that they were due to the waterLOGSY effect. This observation indicated the external location of the PEG regions and internal location of the aliphatic chains, supporting the hypothesized envelope bilayer architecture.

adequately combined (8:1 mass ratio) and added, LAE molecules supposedly interacted with the nanocomplexes, while their aggregation was prevented by the subsequent attachment of PEGst molecules. In fact, the overall neutral ZP of the resultant enveloped nanocomplexes suggested that the hydrophilic PEG portions of PEGst were oriented toward the outer media. The interaction of both surfactants would hypothetically occur through their hydrocarbon chains, constituting a surfactant bilayer (Fig. 3A).

To confirm this hypothesis, $^{1}$H NMR analysis (Fig. 3B, S4 and S5) and water-ligand observed via gradient spectroscopy (waterLOGSY) experiments (Fig. 3B and S6) were carried out on the enveloped nanocomplexes, where bulk solvent ($H_2O$) protons were selectively saturated, and this magnetization was transferred via cross-relaxation to free molecules in contact with water media. As a result, the resonances of molecular regions interacting with water appeared with opposite signs to those interacting within a structure, such as a nanoparticle [43]. The resulting spectrum (Fig. 3B) clearly showed a 3.71 ppm inverted peak corresponding to the PEG regions of PEGst, confirming their external location on the nanocomplex surface in contact with the aqueous medium and with higher mobility compared to the stearate region. On the

other hand, the signal corresponding to bulk aliphatic chains from both PEGst and LAE (1.27 ppm) remained noninverted, indicating their internal location within the structure. Altogether, these results supported the hypothesized envelope bilayer architecture, where PEG regions remain oriented toward the external aqueous media, while aliphatic chains from both surfactants are located inside the nanostructure.

### 2.4. *In vitro performance of enveloped nanocomplexes and their potential for scalability and translation*

The high ionic force and complex composition of intestinal fluids represent one of the barriers for oral delivery, where adequately tuning the nanoparticle surface may drastically determine the capacity of the carriers to maintain their physicochemical properties under physiological conditions [44,45]. The evaluation of our nanocomplexes in biorelevant fluids revealed that their enveloping shell provided adequate colloidal stability [44] (Fig. 4A), while protection against enzymatic degradation (Fig. 4B) and sustained release (Fig. 5C) were attributed to Zn because of its enzymatic inhibitory [46] and insulin complexation [24,47] properties, respectively. Additionally, the batch size was increased by 100-fold (Fig. 1E), indicating the successful identification and control of key process control parameters. Notably, scaling-up potential constitutes a highly important added value that current nanotechnology-based drug delivery approaches rarely have [48,49].

In addition, given the particularities of the insulin-Zn interaction, the possibility of translating this technology to other biomacromolecules was uncertain. Thus, we explored the nanocomplexation of an RNA model molecule with biometals by adapting the production procedure and the biomolecule–biometal mass ratios. Nanocomplexes with tunable surface charges coated with several polymers were obtained (Table S5, S6 and S7), offering possibilities for the further modulation of nanocarrier properties. While the preliminary character of these studies is noted, the results suggest that producing coated nanocomplexes of biometals and biomacromolecules is feasible, which opens up new avenues for formulation development based on this strategy. Particularly, exploring combinations of biomacromolecules and biometals between which specific physiological interactions are known to take place could be an approach of interest.

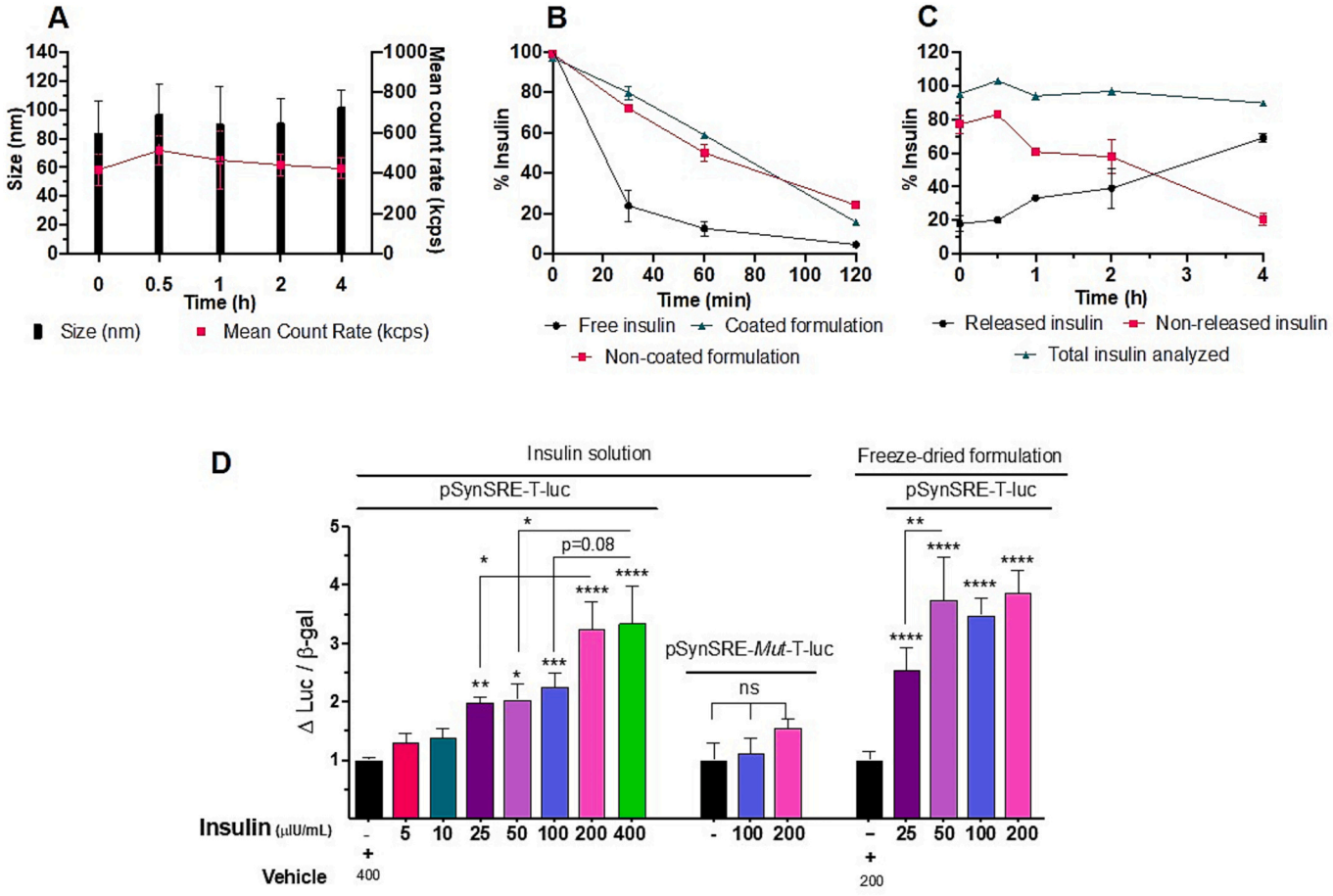


**Fig. 4.** In vitro physicochemical characterization of the coated nanocomplexes. A, Colloidal stability of enveloped nanocomplexes as a function of average particle size and count rate measured by DLS (mean value ± S.D. ($n = 3$)). The formulation proved to be stable for up to 4 h, as opposed to the noncoated nanocomplexes, which immediately aggregated (data not shown). B, Protection of insulin against pancreatic degradation as a function of remaining nondegraded insulin. Both coated and noncoated formulations displayed similar profiles, increasing insulin $t_{1/2}$ by 4-fold with respect to that of free insulin (mean values ± SDs (n = 3)). C, Insulin release from coated nanocomplexes. A sustained release over the incubation time (up to 4 h) was displayed (mean values ± SDs (n = 3)). D, Insulin bioactivity evaluation in pSynSRE-T-luc-transfected cells as a function of luciferase activity over a transfection control promoter (beta-galactosidase). Fresh solutions of free insulin of increased concentrations as a positive control induced dose–response luciferase activity in pSynSRE-T-luc-transfected cells, while no statistically significant effect was observed in pSynSRE-Mut-T-luc-transfected cells, bearing four-point mutations in the insulin-responsive element, therefore validating the assay. Reconstituted freeze-dried coated nanocomplexes at insulin concentrations equivalent to those of the positive control resulted in the specific activation of the insulin receptor, shown as delta luciferase, compared to the control. The luciferase activity values obtained were in the same range as those obtained with fresh insulin solutions, confirming the preserved bioactivity of insulin after formulation processing and freeze-drying. Cell study results are presented as the means ± SDs, $n = 5$ independent experiments with 6–8 replicates per condition in each (one-way ANOVA followed by Tukey's multiple comparison test; significance levels compared to the control $^{*}p \leq 0.05$; $^{***}p \leq 0.001$, $^{****}p \leq 0.001$).

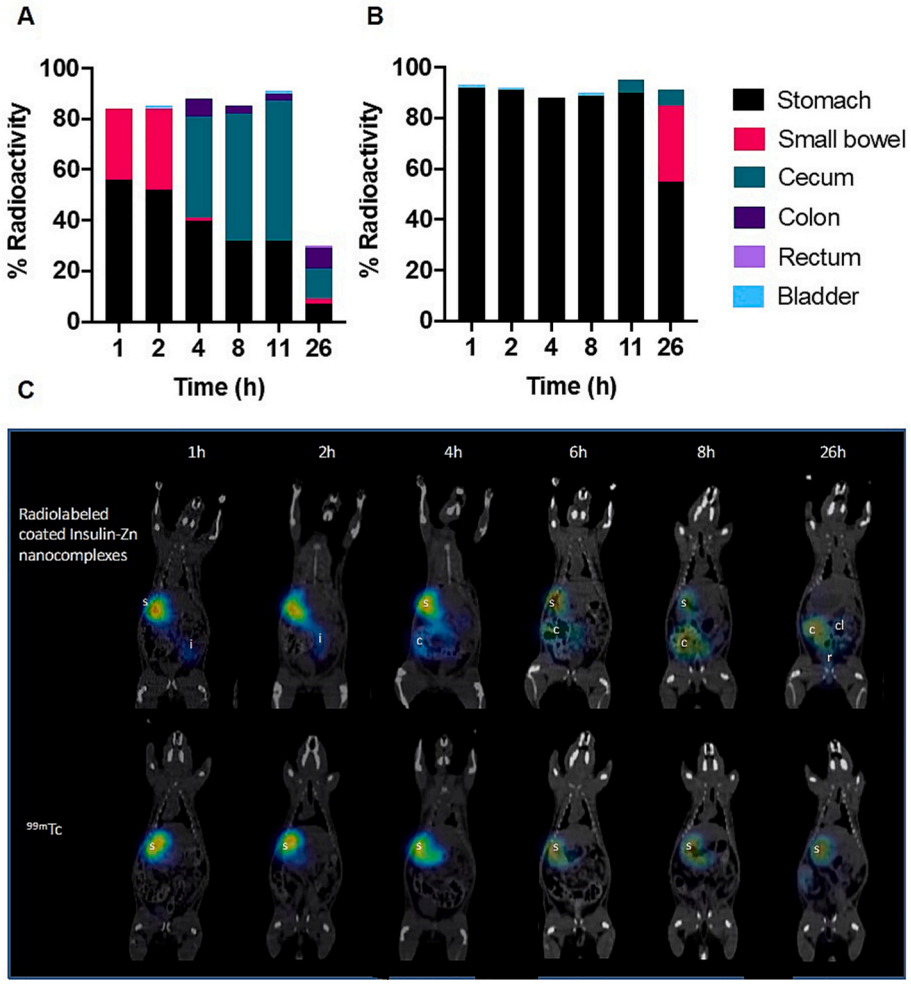


**Fig. 5.** Biodistribution of technetium-99 m radiolabeled nanocarriers in rats. A, % Radioactivity detected per organ after oral administration of the radiolabeled formulation. B, % Radioactivity detected per organ after oral administration of [$^{99m}$Tc]-sodium pertechnetate (control). C, SPECT-CT images of the rats after oral administration of the radiolabeled formulation and free $^{99m}$Tc control; s = stomach; I = intestine; c = cecum; cl = colon; r = rectum. The radiolabeled carriers remained mostly in the small bowel (up to 2 h) and in the cecum (4 h, 8 h and 11 h) for the duration of the study, whereas the free technetium control remained in the stomach. The results are presented as the mean values of $n = 4$.

An ultimate constraint specific to oral administration arises from the necessity to generate a solid dosage form as the end product. This usually requires the freeze-drying of formulations produced in aqueous-based media, which may compromise the preservation of the initial physicochemical properties of nanoparticles as well as the bioactivity of the loaded drug [17,50]. To assess whether the lyophilized nanocomplexes maintained their key properties, samples from freeze-dried, small and large batches were evaluated in vitro, showing preserved insulin bioactivity on human INSR in human HepG2 hepatocytes [51,52] (Fig. 4D) and physicochemical properties (Fig. S2) after 2 months of storage.

Next, the freeze-dried nanocomplexes were loaded into gelatin capsules along with a composition intended to generate carbon dioxide ($CO_2$) gas bubbles that would promote a fast resuspension of the nanocomplexes and their projection toward the intestinal wall, comprising tartaric acid (TA), sodium bicarbonate (SBC) and Poloxamer 199 (P188). This acid-base reaction has been employed in a similar approach using citric acid and SBC to promote tablet disintegration [53,54]. It was also employed to promote the in situ assembling and/or stabilization of nanostructures [55–57], where intestinal permeation was ultimately dependent upon the action of permeation enhancers such as trimethyl chitosan (TMC) [54] or sodium dodecyl sulphate (SDS) [55–57] or the performance of nanocarriers [53] in this composition, TA and SBC were selected to generate the $CO_2$ bubbles, P188 was employed as surfactant to decrease surface tension and therefore increase the intensity of the reaction effect [58], and intestinal permeation was expected to be attained on account of the rationally designed nanocomplexes. The capsules were further coated with an enteric polymer to prevent gastric degradation, and the integrity of the coating and the triggering of the gas producing reaction after coating dissolution were assessed in simulated gastric and intestinal fluids respectively. In the latter, the acid-base reaction was observed to take place within 2 min upon coating dissolution, with an intense gas production (Fig. S7). The capsules were stored at RT protected from humidity up to 1.5 months before administration to pigs, when their content homogeneity and drug bioactivity was previously evaluated by s.c. administration to healthy rats.

### 2.5. *In vivo interaction of enveloped nanocomplexes with the intestinal wall*

The nanocarriers were radiolabeled with technetium-99 m ($^{99m}$Tc) via linkage to the PEG chains on the nanocarrier envelope [59], followed by oral administration to rats and subsequent single photon emission computed tomography-computed tomography (SPECT-CT) evaluation [60]. Prior to the study, the stability and lack of release of the radioisotope in simulated gastric fluid (SGF) were assayed (Fig. S8 and S9).

The results (Fig. 5) showed that, while the free technetium control (sodium pertechnetate solution) remained localized in the stomach, the

radiolabeled carriers remained mostly in the small bowel (up to 2 h) and cecum (4 h, 8 h and 11 h) for the duration of the study. This prolonged intestinal transit profile is in agreement with similar experiments carried out with nanoparticulate formulations [59,61] and is supported by the lower transport velocity in distal segments of the gastrointestinal (GI) tract [62] and the fact that isoflurane anesthesia is known to decrease GI motility and prolong transit times due to muscle relaxation [63]. Overall, the $^{99m}$Tc-labeled formulation significantly interacted with the intestine, having been retained for up to 26 h, in contrast to the technetium solution control, which remained mostly in the stomach. This enhanced intestinal interaction of the formulation could be attributed to the nanocarrier features, namely, i) their small size for favoring cellular interactions and mucodiffusion [32]; ii) a PEGylated surface for facilitating mucodiffusion [38]; and iii) the presence of LAE, a surfactant with a shown capacity to disrupt cellular membranes [42], hypothetically potentiated by PEGst. For instance, PEG-fatty acid esters have shown enhanced skin drug penetration [64], while other nonionic polyoxyethylated surfactants have been widely studied as topical ocular penetration enhancers [65]. Interestingly, no systemic absorption of $^{99m}$Tc was observed. This lack of absorption of the nanosystem was expected based on previous literature pertaining to nanoparticle transport across the intestinal wall. The key issue was whether the enhanced interaction of the nanosystem with the intestinal wall may be translated into greater insulin absorption. The absence of the systemic absorption of the nanosystem itself may be considered a positive feature in terms of pharmaceutical purposes, since it would seem to imply reduced toxicological concerns [61].

### 2.6. Pharmacological performance of the enveloped nanocomplexes

The enveloped nanocomplex efficacy was first evaluated following subcutaneous (s.c.) administration to healthy rats [44] (Fig. 6A).

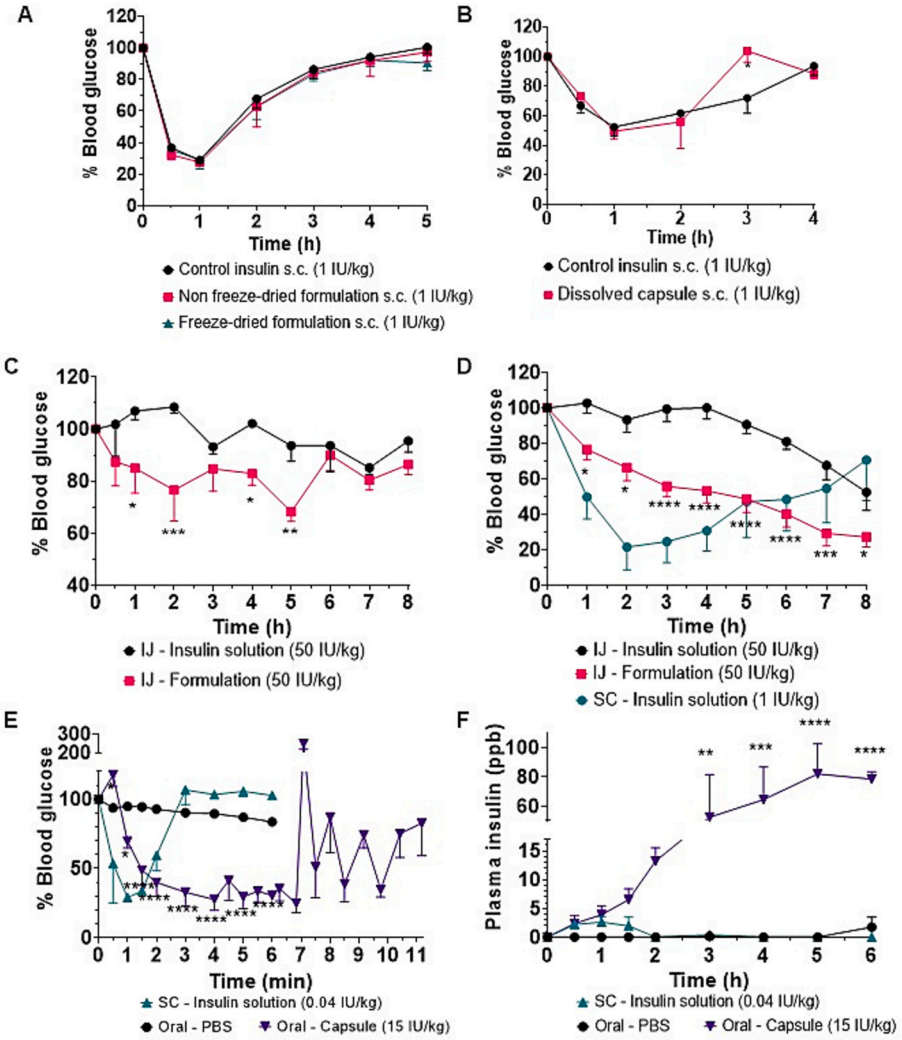


**Fig. 6.** In vivo efficacy evaluation in small and large animal models. Efficacy results are displayed as % blood glucose values with regard to the baseline values at time 0 h. Plasma insulin results are displayed as plasma insulin concentrations (ppb (ng/L)). A, Blood glucose after s.c. administration of freshly prepared and freeze-dried reconstituted formulation, vs. insulin control to healthy rats. B, Blood glucose after s.c. administration of insulin extracted from enteric capsule powder after 2 months of storage vs. insulin control to healthy rats. C, Blood glucose profile after IJ administration of the formulation ($n = 5$) vs. an insulin solution (negative control) ($n = 6$) to healthy rats. D, Blood glucose profile after IJ administration of the formulation ($n = 9$) vs. an insulin solution (negative control) ($n = 8$) to diabetic rats. E, Blood glucose profile after oral administration of enteric capsule formulation vs. oral administration of PBS (negative control) and SC administration of an insulin solution (positive control) ($n = 3$) to awake domestic pigs. Oscillations in levels from 6 h onward were due to i.v. administrations of glucose in response to hypoglycemic shock signs. F, Plasma insulin analysis by LC–MS resulting from the administration of the enteric capsule vs. negative and positive control to awake domestic pigs. No plasma samples were withdrawn after 6 h due to concern about the healthy state of the animals. All results are displayed as the mean values ± SEMs. A two-way ANOVA followed by a Holm–Sidak multiple comparison test was applied; significance levels compared to the control *$p \leq 0.05$; **$p \leq 0.01$; ***$p \leq 0.001$, ****$p \leq 0.001$).

Subsequently, the formulation was assayed for its efficacy in vivo by intestinal direct injection [44,66–69], which avoids the variability associated with gastric transit times, both in healthy and diabetic rats [69]. The healthy rat model maintains the physiological insulin autoregulation mechanisms [70] and avoids the high variability associated with STZ diabatization [68,71]. As a counterpart, only modest responses are to be expected [44,68], and fasting periods need to be decreased [69]. Hence, the intrajejunal (IJ) administration of the coated nanocomplexes to healthy rats (Fig. 6C) yielded an expected modest, but significant, 42 % decrease in the initial blood glucose levels. Importantly, the effect was maintained for up to 6 h. Similar responses were reported for other delivery carriers [68,72,73]. This finding confirmed that the insulin associated with the nanocarrier was absorbed in a sufficient amount to exert a prolonged blood glucose reduction response [68,70,74]. Hypothetically, this could be due to the enhanced nanostructure interaction with and penetration into the intestinal epithelium, as noted for the radiolabeled formulation.

On the other hand, β-cell deficiency in the diabetic model allows low amounts of absorbed insulin to elicit a markedly decreased glucose response [68], and hence, potential effects of an oral formulation would have a higher chance of being identified. Following direct IJ injection of the formulations, a remarkable blood glucose decrease of up to 80 % was obtained (Fig. 6D), with clear differences regarding the negative control even at the end of the measurement period (8 h). This high and prolonged response was comparable to or higher than those reported in references in the field [75–77]. As expected, the results showed a clearer effect in comparison with those of the healthy rat model, further confirming insulin intestinal absorption. Along with biodistribution studies, the results indicated that the nanocomplexes enabled insulin absorption without nanocarrier translocation.

### 2.7. Preliminary assessment of the lack of chronic immunotoxicity in mice

Chronic exposure to insulin treatment requires the consideration of

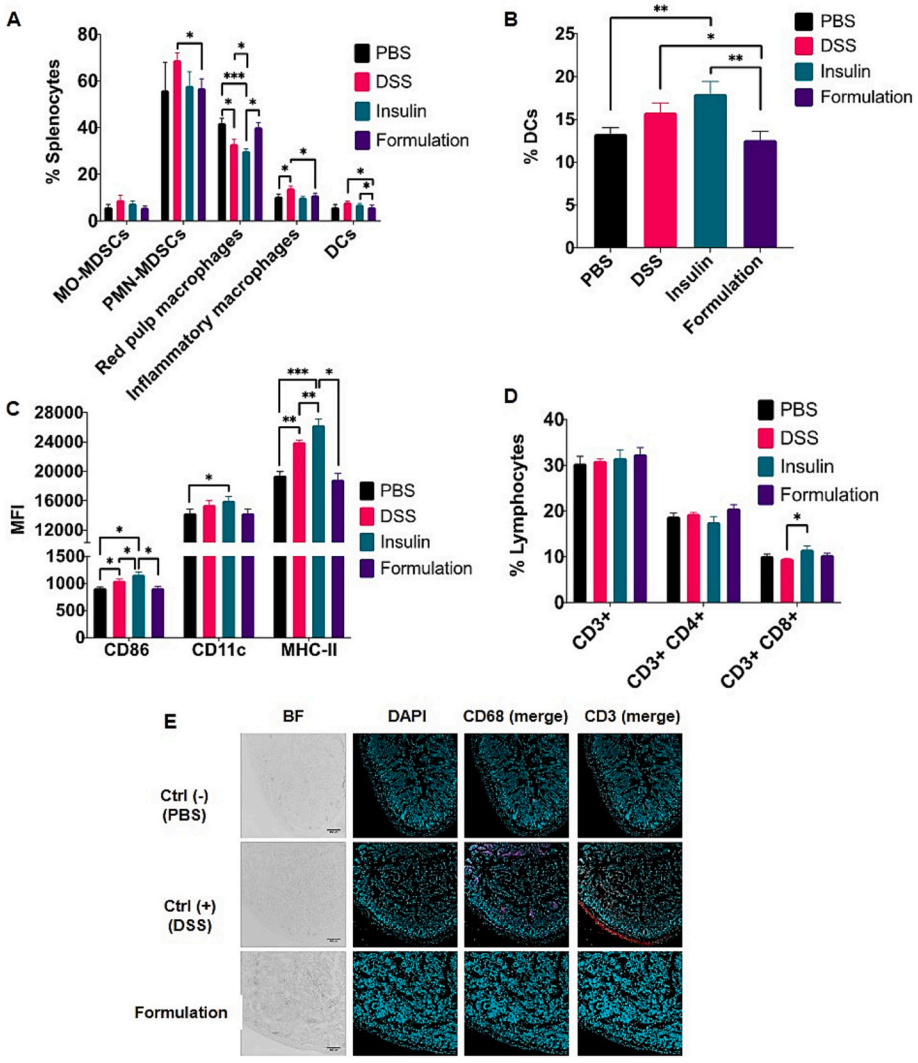


**Fig. 7.** Preliminary chronic immunotoxicity evaluation of the formulation in mice. The results from FACS analysis of the immune inflammatory status of lymphoid organs after 28 days of treatment. A, Percentage of myeloid cells in spleens following chronic administration of formulation vs. insulin for up to 28 days. Different myeloid subpopulations (inflammatory monocytic MDSCs (MO-MDSCs), granulocytic-MDSCs (PMN-MDSCs), macrophages and dendritic cells (DCs)) were evaluated for each treatment group. B, Evaluation of DC maturation after formulation vs. insulin administration in terms of percentage. C, Evaluation of DC maturation in terms of fluorescence intensity for each treatment group. D, Percentage of lymphocytes after chronic administration of formulation vs. insulin; percentage of T lymphocytes CD3 total, CD4 or CD8. The T-cell percentages from each treatment group were similar. E, Immunohistochemistry of intestinal regions after formulation administration with CD3 and CD68. In the Fig., colocalization with DAPI is reported (magnification 20× with dry objective). No increases in lymphocyte (CD3) or macrophage (CD68) signals were observed at the level of the small intestine after chronic administration of insulin (data not shown) or the nanocarriers. Bar graphs represent the means ± SDs; $n = 5$ mice per group. *$p \leq 0.05$; **$p \leq 0.01$; ***$p \leq 0.001$, by one-way ANOVA.

potential adverse effects, such as an inflammatory response at the GI tract level [78]. Hence, the potential activation of inflammatory processes following chronic exposure (28 days) to a high dose of the formulation was assessed via the morphological analysis of treated intestine and evaluation of immune cell populations. Altogether, the results of the formulation group were found to be almost equal to those of the negative control group (Fig. 7). Notably, the increase in mature dendritic cells (DCs) may be indicative of partial inflammation elicited by chronic insulin administration (Fig. 7B, C). Interestingly, the nanocarriers did not exert this effect and presented levels of CD86 on DCs and MFI levels for the markers evaluated similar to the negative control group (Fig. 7B, C), indicating that the protein encapsulation within the nanocarrier led to the protection of the intestine against the deleterious effect of the protein. Overall, the results from this preliminary immunotoxicology evaluation indicated that the tested nanocarriers can be considered potentially safe and that they were able to mitigate the proinflammatory activity of the administered free-form insulin. Further advanced toxicological studies are needed to determine the formulation safety.

### 2.8. *Oral dosage in capsule form elicited high absolute oral bioavailability in healthy awake pigs*

A preliminary study on a final oral enteric capsule dosage formulation in pigs as a large animal model was conducted. Prior to efficacy studies, the preserved bioactivity and dose uniformity of the insulin dose contained in the capsules after up to 2 months of storage was confirmed by s.c. injection into rats and blood glucose monitoring (Fig. 6B).

Interestingly, upon oral administration of the enteric capsule formulation, a fast, profound, and sustained blood glucose reduction was obtained (Fig. 6E), attaining blood glucose values that were 29 % of the initial values. LC–MS analysis of the insulin in plasma samples revealed that animals treated with the capsule formulation presented much higher levels than those treated with the s.c. insulin control (Fig. 6F). Area under the curve (AUC) analysis corresponding to the first 6 h of the study (Table S8) revealed a 21.0 % absolute bioavailability. Given that no plasma samples were withdrawn after 6 h, this 21 % value might have been underestimated. This outstanding bioavailability value should be cautiously taken into consideration given the limited number of pigs used in the experiment. In fact, only physical permeation-enhancing devices have recently been reported to result in bioavailability values from 10 % to near 100 % in swine [10–13]. Moreover, the only two currently approved drug delivery formulations for peptide systemic oral absorption, both based on the use of penetration enhancers, resulted in a 1.22 % GLP-1 bioavailability in dogs [15] and 0.8 % in humans [79] (Rybelsus®) and 0.7 % octreotide bioavailability in humans [16] (Mycapssa®). In addition, recent preclinical studies in large animal models with several formulations have reported bioavailability values ranging from 1.2 % to 16 % for octreotide [80–83] and 2.54 % for a GLP-1 receptor agonist [80]. Nevertheless, it should be noted that the peptide molecular weight is a key determining factor for oral bioavailability potential, followed by other factors, such as stability, hydrophobicity, net charge, and chemical configuration [84,85]. For instance, the same technology leading to 16 % octreotide bioavailability in pigs was simply translated into 1.9 % insulin bioavailability [86]. Notably, this preliminary study presented low intervariability among the three animals tested (Fig. 6E and F), which usually represents a challenging aspect in formulation and device development [10,11,80,87].

Dose–response studies, as well as the evaluation of additional formulation controls, are necessary before advancing the evaluation and development of this formulation. Nevertheless, the promising results from this exploratory evaluation are encouraging for the continued development and evaluation of coated insulin-Zn nanocomplexes in an advanced preclinical setting.

## 3. Conclusions

Here, we disclose the design and development of orthogonal-shaped Insulin-Zn nanocrystals, enveloped by a well-organized bilayer composed of GRAS and FDA-approved materials, with penetration enhancing and stabilizing properties. Despite the apparent complexity, the formulation is highly straightforward to manufacture, enabling its scalability lo large batches of the product. The freeze-dried form of the nanocarriers proved to maintain its properties with full bioactivity of the processed protein. Concerning efficacy, in vivo studies showed that these nanosystems were able to elicit hypoglycemia both in healthy and diabetic rat models, without systemic absorption of the carriers. No toxic effects were observed after a 28-day chronic immunotoxicity study in mice. An enteric capsule dosage form containing the freeze-dried powder of the formulation elicited profound and sustained blood glucose decrease in healthy awake pigs, resulting in over 20 % absolute bioavailability. Successful production of tRNA-biometal nanocomplexes indicated this strategy could be potentially adapted for other biomacromolecules, and the present study would represent the basis for the design and development of further biometal-based nanocarrier prototypes, since these carriers share a common industry-transferable perspective of biocompatibility, scalability and cost-benefit criteria.

## 4. Materials and methods

### 4.1. *Materials*

Recombinant human insulin hexamer Insuman® (5808 Da Mw) was kindly provided by Sanofi (Paris, France). Pharmaceutical grade Zn acetate dehydrate (EMPROVE®) was obtained from Merck Millipore (Germany). HCl and NaOH solutions, acetic acid and trifluoroacetic acid were purchased from Scharlau (Barcelona, Spain). Food grade (GRAS) lauroyl arginate ester (LAE, ELA, MIRENAT® P-100, E-243) was obtained from Vedeqsa Inc. (Barcelona, Spain). Pharmaceutical grade polyethylene (40) stearate 40 (PEGst) was acquired from Croda (UK). Pharmaceutical grade trehalose was purchased from Pfanstiehl, Inc. (Waukegan, IL, USA). 5-FITC and NHS-Cy5 were obtained from Embalech (Berlin, Germany). Gelatin T00 capsules were purchased from Torpac Inc. (Fairfield, NJ, USA). Eudragit L100 was a kindly gifted by Evonik (Essen, Germany). Sodium perchlorate monohydrate, mannitol (USP grade), pancreatin from porcine pancreas (4 USP), tRNA from baker's yeast, iron(III) chloride hexahydrate (ACS reagent, 97 %), insulin from bovine pancreas (≥25 USP units/mg (HPLC), powder) and streptozotocin (STZ) were acquired from Sigma–Aldrich (Madrid, Spain). Polyvinyl alcohol (PVP) was obtained from Basf (Barcelona, Spain). Ultrapure DNAse-/RNAse-free distilled water was purchased from Gibco (Life Technologies, Madrid, Spain). Polyethyleneglycol (5 kDa Mw)-polyglutamic acid (10 units) copolymer (PEG(5 k)-PGA(10)) and poly-l-arginine (PARG) (26–37 kDa Mw) were purchased from Polypeptide Therapeutic Solutions (PTS, Valencia, Spain). PROTASAN (chitosan) was acquired from FMC (Novamatrix) (Sandvika, Norway). Chondroitin-6-sulfate sodium salt (CS) was obtained from Fluka (Fisher Scientific SL, Madrid, Spain). Sodium hyaluronate (HA) (research grade, 41 kDa-65 kDa) was purchased from Lifecore Biomedical, LLC (Chaska, MN, USA). Colominic acid sodium salt (polysialic acid, PSA) was obtained from Nacalai Tesque Inc. (Tokyo, Japan). Water SpS was purchased from Romil Ltd. (Cambridge, UK). Sodium chloride (RFE, USP, pH. Eur) and Tin(II) chloride ($SnCl_2$) were obtained from Panreac (Barcelona, Spain). Physiological serum (NaCl 0.9 % *w/v*) was purchased from Braun (Hessen, Germany). Ultrapurified water was obtained from a Millipore Milli-Q Plus water purification system (Darmstadt, Germany). All the other chemicals were of analytical grade.

Regarding the materials employed for cell bioactivity studies, Eagle's minimum essential medium (EMEM) growth medium (1 g glucose/L) was purchased from SIGMA (UK), Fetal bovine serum (FBS) was acquired from GIBCO, Thermo (South America), nonessential amino acids

were obtained from GIBCO, Thermo (Grand Island USA), 2 mM L-glutamine was acquired from Sigma (Brazil), penicillin–streptomycin was obtained from Sigma (Israel), and trypsin solution was purchased from Sigma (USA). Viafect was obtained from Promega (Madison USA), Turbofect was purchased from Thermo (Lithuania), pMAXGFP was acquired from Lonza (Köhln Germany), and pSynSRE-T-luc and pSynSRE-Mut-T-luc were obtained from Addgene (Cambridge USA). Hoechst 33258 and Type I collagen solution in phosphate-buffered saline (PBS) were obtained from Sigma (Israel).

With regard to materials used for in vivo efficacy studies in pigs, Calypsol (Ketamine) was purchased from Gedeon Richter PLC (Hungary), Dexdomitor (Dexmedetomidin-HCl) was acquired from Orion Corporation (Finland), xylazine was provided by Produlab Pharma (Netherlands), Forane (Isoflurane) was acquired from Rompharm Company (Romania), Braunol (Povidone-iodine) was purchased from B. Braun Medical AG (Germany), Heparibene NA (Heparin) and Salsol (Isotonic Saline) were obtained from TEVA Ltd., (Hungary), Euthazol (Pentobarbital NA) was acquired from Produlab Pharma BV (The Netherlands), Formalin (4 %, buffered) was obtained from Sigma–Aldrich Co. (US), Syvaquinol was provided by Laboratorios Syva S. A., and Rheumocam was purchased from Chanelle Pharm. ML.

The HepG2 cell line was obtained from ECACC (UK, distributed by SIGMA) and cultured in growth medium (EMEM supplemented with 10 % FBS, 1 % nonessential amino acids, 2 mM L-glutamine, and 1 % penicillin–streptomycin). Cells were passaged once per week by trypsinization (10× Trypsin solution) for 5 min and passaged through an 18-gauge needle to obtain a single-cell suspension. They were obtained between passages 3 and 20.

For the in vivo biodistribution studies with radiolabeled nanocarriers, male Wistar rats (250 g) were housed and cared for under standard conditions with access to water and food ad libitum. All procedures were performed following previously approved protocols according to the Ethical and Biosafety Committee guidelines from the University of Navarra. For the in vivo efficacy studies, male Sprague–Dawley rats (250–300 g) were obtained from the Central Animal House, University of Santiago de Compostela (Spain). They were kept under 12 h light/12 h dark cycles and fed a standard laboratory rodent diet (Panlab A04, Panlab laboratories). All animal experiments were reviewed and approved by the ethics committee of the University of Santiago de Compostela (ref. 1500AE/12/FUN01/FIS02/CDG3) according to the European and Spanish regulations for the use of animals in animal studies and were therefore performed in compliance with Directive 2010/63/EU of the European Parliament and Council. For the in vivo immunotoxicity studies, 8-week-old female BALB/c mice (25 g) obtained from Harlan (San Pietro al Natisone, Italy) were housed and cared for under standard conditions with access to water and food ad libitum, and all animal experiments were approved by the local animal ethics committee at the University of Padova and were performed in accordance with governing Italian law and EU directives and guidelines.

In vivo efficacy studies of pigs were conducted on 12- to 14-week-old neutered male domestic pigs (*Sus scrofa domesticus*) (15–20 kg) from the Research Institute of Animal Breeding and Nutrition, Herceghalom, Hungary. They were housed in individual caging (1 m × 2.5 m), fed a standard powder diet for domestic pigs twice a day with access to water ad libitum and allowed to acclimatize for 1 week prior to the study.

The studies were designed in accordance with accepted pharmacological principles to meet the requirements of the principles of Hungarian Act 1998: XXVIII regulating animal protection (last modified by Act 2011 CLVIII) and the Government Decree 40/2013 on animal experiments; EEC Directive 2004/27/EC of the European Parliament and of the Council of March 31, 2004 amending Directive 2001/83/EC on the Community code relating to medical products for human use (Official Journal L-136, 30/04/2004, pp. 34-57). Animal handling and care were conducted according to the Guide for the Care and Use of Laboratory Animals, NRC, 2011 and Directive 2010/63/EU (European Parliament and Council, took full effect on 1 January 2013). Special permission for animal studies under number PEI/001/3948-6/2014 was issued by the Pest County Government Office of Food Safety and Animal Health Directorate. All procedures carried out on animals were approved by the local ethical committee of Semmelweis University.

### 4.2. Methods

#### 4.2.1. Production of enveloped insulin-Zn nanocomplex formulations

First, insulin-Zn nanocomplexes were fabricated in a two-step procedure consisting of inducing the interaction between insulin and Zn by pH adjustment followed by dispersion of the complex material in buffer media. To this aim, a 1.5 mg/mL insulin solution in 0.05 N HCl was mixed with a 20 mg/mL Zn acetate aqueous solution at a 1:6 M ratio, and the solution pH was adjusted to 5.4 by the addition of 0.1 N NaOH under magnetic stirring at 300 rpm, inducing coprecipitation of the components. Next, this mixture was incubated at 4 °C [88] for 3 h to allow for the crystallization of the protein–metal complex. After the incubation period, the complex material was allowed to temper at RT for 4 min, resuspended by vortexing (20 s) and poured over10 mM PBS under magnetic stirring at 300 rpm and a 1:1 volume ratio for 30 s to obtain a colloidal nanocomplex suspension (final insulin concentration of 0.75 mg/mL).

To stabilize the nanocomplexes, a surface coating comprised of LAE and PEGst was applied. To this aim, the colloidal nanocomplex suspension was maintained under magnetic stirring at 300 rpm, while a 10 % *w/v* aqueous solution of PEGst and a 1 % w/v aqueous solution of LAE were subsequently and dropwise added at an 8:1 PEGst:LAE mass ratio, for a final 1.15:8:1 nanocomplexes:PEGst:LAE mass ratio. This mixture was maintained under magnetic stirring (300 rpm) for 10 min and then allowed to equilibrate for 5 min before further characterization.

For the 20-mL final volume batches, magnetic stirring was increased to 500 rpm, and glassware was adapted while maintaining constant production conditions. For the 200-mL final volume batches, magnetic stirring homogenization and vortexing were substituted by paddle homogenizing (300 rpm, IKA® RW 20 digital, S28N-18G dispersing tool, IKA®-Werke GmbH & Co. KG, Staufen, Germany), adequately adapting the glassware size and keeping the rest of the production conditions constant.

For short- and long-term storage periods before use, the formulation was converted into a dry powder by freeze-drying with trehalose as a cryoprotectant. For this purpose, a previous screening of cryoprotectants and their concentrations was carried out, from which the best performing combinations and concentrations were selected in terms of the maintenance of formulation properties upon lyophilization along with minimizing the amount of incorporated cryoprotectant. Trehalose was selected because it is a widely employed and characterized cryoprotectant, enabling an accurate evaluation of the freeze-dried product and comparison with reported lyophilized formulations in the literature. However, a polyvinyl alcohol (PVP) and mannitol mixture was also employed as a nonglycemic alternative, given the reported glycemic effect of trehalose, albeit at a lower and steadier rate than glucose [89]. Finally, the coated nanocomplex suspension was mixed with a 10 % *w/v* trehalose solution at equal volumes under magnetic stirring (300 rpm) to yield a nanocarrier suspension in a 5 % w/v trehalose medium. Alternatively, the coated nanocomplex suspension was mixed with 0.25 % w/v PVP and 9 % w/v mannitol solution at equal volumes under magnetic stirring (300 rpm) to yield a nanocarrier suspension in 0.125 % w/v PVP and 4.5 % w/v mannitol medium. In both cases, the final suspension was immediately frozen at -80 °C and subsequently freeze-dried (Genesis VirTis 25EL pilot lyophilizer). The obtained powder product was stored at RT in a desiccator. For reconstitution, ultrapure water was added to the freeze-dried product in a volume corresponding to the initial nanocomplex concentration before mixing with the cryoprotector, followed by 30 s of vortexing. Physicochemical and in vitro performance evaluations were performed on the reconstituted nanocomplexes to evaluate the maintenance of the performance observed for

the freshly produced formulation.

For the preparation of the enteric capsule with gas-aided resuspension and propulsion of the nanocomplexes, the freeze-dried product with the PVP and mannitol combination was previously mixed with a powder mixture of bubbling agents at a 1:1 weight ratio. More specifically, the mixture of bubbling agents contained tartaric acid (TA), sodium bicarbonate (SBC) and Poloxamer 188 (P188) at a 5:4:1 weight ratio. TA was employed as substitute for citric acid, commonly employed for the generation of carbon dioxide upon reaction with SBC in pharmaceutical compositions [54,56], and the mass ratio was adjusted so as to maintain the molar ratio of the acid and carbonate groups involved in the acid-base reaction. P188 was included due to the key role of surfactants in the explosiveness of the reaction, which decrease surface tension and thus the work required for bubble formation [58]. Following, T00 gelatin capsules (Torpac Inc., Fairfield, NJ, USA) were filled with the formulation powder containing the nanocomplexes and the bubbling agents and subsequently coated with an Eudragit L100 solution 10 % *w/v* in a 1:1 mixture of acetone and isopropanol with the aid of a ProCoater 1.3 (Torpac Inc., Fairfield, NJ, USA). Three coating polymer layers were deposited on the capsules by alternatively immersing each side in the coating solution for 10 s and subsequently drying for 30 min. To evaluate the integrity of the coating, capsules were immersed for 2 h in 20 mL [90] SGF at 37 °C under horizontal shaking (300 rpm, Heidolph Instruments GmbH & Co. KG, Schwabach, Germany) and checked for the lack of release, and subsequently immersed into 50 mL of SIF and checked for coating dissolution within 20 to 30 min, triggering content release and gas production. For storage, the capsules were kept in closed containers in a dry environment with the aid of silica beads.

#### 4.2.2. Nanocarrier labeling

To fluorescently label the nanocarriers for subsequent tracking in cell studies, insulin was covalently labeled with either 5-FITC or NHS-Cy5 prior to its complexation into nanocarriers. For this purpose, insulin was dissolved in 0.1 M bicarbonate buffer at a pH of 8.58 and concentration of 10 mg/mL. To obtain FITC-insulin, 100 μL of a 10 mg/mL solution of 5-FITC in ethanol was added to 1 mL of the previous insulin solution under magnetic stirring (300 rpm). For the production of Cy5-insulin, 10 μL to 100 μL of an NHS-Cy5 solution in DMSO at concentrations ranging from 0.01 mg/mL to 10 mg/mL was added to 1 mL of the previous insulin solution under magnetic stirring (300 rpm) to obtain different labeling degrees. Next, the mixture was allowed to react for 1 h in the dark and then purified in a gel filtration column (Centri Pure P10, emp Biotech GmbH, Berlin, Germany). To remove buffer salts, the labeled insulin was then precipitated by pH adjustment at its pI and centrifuged (7000 *g*, 4 °C, 15 min, Eppendorf Centrifuge 5430 R, Eppendorf Ibérica S.L.U., Madrid, Spain). The supernatant was discarded, and the pellet was resuspended in ultrapure water and freeze-dried (Genesis VirTis 25EL pilot lyophilizer). The amount of FITC or Cy5 labeled with insulin was calculated by HPLC insulin quantification and FITC or Cy5 fluorescence measurement (Multimode microplate reader Synergy H1 Biotek, Isaza Scientific, Madrid, Spain) using the same sample. The freeze-dried labeled insulin was incorporated into the nanocomplexes by substituting plain insulin in the nanocomplex production described above and increasing the amount of PEGst in the coating from the 8:1 PEGst:LAE mass ratio to 12:1.

#### 4.2.3. Physicochemical and morphological characterization

Particle size distribution and PDI were determined by DLS, and the ZP was determined from the electrophoretic mobility values obtained by laser Doppler anemometry (LDA) using Malvern Zetasizer equipment (NanoZS ZEN 3600, Malvern Instruments, Worcestershire, UK) equipped with a red laser light beam ($\lambda = 632.8$ nm). The formulation was directly measured without dilution at 25 °C with at least three different batches and triplicate analysis of each batch. For the Cy5-labeled samples, particle size was measured by nanoparticle tracking analysis (NTA) using Malvern Nanosight equipment (Nanosight NS300 Malvern Panalytical Ltd., UK) with Nanosight NTA Software (v3.3 (PSS0235-13)). The formulation was measured at a 1:10 dilution in ultrapure water at 25 °C in triplicate, with 5 measurements of 60 s per sample and a continuous syringe pump flow of 50 μL/min. The morphological evaluation of the formulation was carried out using a transmission electron microscope (TEM, CM12, Philips, Netherlands), for which samples were placed on copper grids and stained with phosphotungstic acid (2 % *w/v* in 500 mM buffer acetate pH 5.5, to avoid nanocomplex dissociation at an acidic pH) for 2 min and allowed to dry overnight in a desiccator.

#### 4.2.4. Insulin association efficiency and loading capacity

The association efficiency (AE) of insulin with the nanocomplexes was analyzed upon separation of the nanocomplexes from the suspending aqueous medium followed by direct and indirect analysis. To this aim, 1 mL of formulation was ultracentrifuged (Beckman Coulter, Optima L-90 K, Brea, USA, rotor 70.1Ti) at 70,000 rpm (average RCF 336,140 g) for 3 h at 15 °C, from which a nanocomplex sediment separated from the suspending medium was obtained. In the case of the freeze-dried and reconstituted formulations, the centrifugation time was increased to 6 h due to the presence of trehalose in the sample (10 % *w/v*), which delayed nanocomplex precipitation due to the increased density of the suspension media. After separating the supernatant, the pellet was dissolved in TFA 0.1 % *v*/v, inducing the dissociation of insulin-Zn complexation due to acidification [20]. Aliquots from both the supernatant (indirect quantification) and the TFA-dissolved pellet (direct quantification) were analyzed by HPLC using a reversed-phase isocratic method as described elsewhere [44,68] (Agilent model, 1100 series LC with diode-array detector set at 214 nm, Santa Clara, USA) with a C18 column (Superspher® RP-18 endcapped) as the stationary phase. The mobile phase was eluted at 1 mL/min and consisted of a 44:56 v/v mixture of phase A (93:7 v/v phosphate buffer (0.1 M, pH 2.3)–acetonitrile) and phase B (43:57 v/v phosphate buffer–acetonitrile). The AE (%) refers to the amount of insulin in the nanocomplexes compared to the initial amount of insulin. The final insulin loading (LC% *w*/w) was calculated by dividing the amount of associated insulin (AE x total insulin in the formulation) by the total weight of the nanocomplexes. For the quantification of the insulin payload (%wt) in the freeze-dried product, a known amount of product was weighed using a precision balance (Kern, model ABT 120-5DM, Kern & Sohn, Balingen, Germany), dissolved in TFA 0.1 % v/v and analyzed by HPLC.

#### 4.2.5. Nanocomplex inner structure characterization by X-ray diffraction

X-ray diffractograms were recorded with an Empyrean diffractometer (PANalytical, The Netherlands) equipped to take measurements of freeze-dried powder samples packed between layers of low-signal Kapton polymer. X-rays were emitted from a sealed tube with a Cu anode ($\lambda(K\alpha 1) = 1.5406$ Å) and collimated prior to irradiating the sample, with optics including a W/Si bilayer mirror. Radiation emitted from the sample was captured with a "PIXcel3D" solid detector. Solid samples were mounted between Kapton layers. Diffractograms were recorded over an angular range of 4–30 degrees, with a 0.02 aperture and 10 s aperture time. The diffractograms were analyzed using HighScore Plus: Version 3.0d".

#### 4.2.6. Structural characterization of the enveloped nanocomplexes by $^1H$ NMR

To assess the nanocomplex coating structure, samples of the final nanocarrier suspension along with separate solutions of each formulation component, at their same concentrations in the final nanocarrier suspension and same dispersion media, were analyzed by $^1H$ NMR. When needed, nanocomplexes were concentrated or purified in 30 kDa Amicon centrifugal filter units (Merck Millipore, Madrid, Spain) (Eppendorf Centrifuge 5430 R, 4000 rcf – 15 °C). NMR spectra were recorded using a Varian Inova 17.6 T spectrometer (Agilent) operating

at a proton frequency of 750 MHz and processed with MestreNova software v10.0.1 referenced with respect to the TMS peak ($\delta = 0$ ppm).

Samples were analyzed in $H_2O$ in thin-wall 5 mm tubes at 25 °C. For deuterium lock and referencing, a glass capillary containing a solution of 0.8 mg of 3-(trimethylsilyl)propionic acid-$d_4$ sodium salt (TSP) in $D_2O$ (99.9 % D) was used. For each sample, a 1D proton spectrum was acquired with strong $H_2O$ signal suppression at ~4.7 ppm using the WaterControl sequence [91]. The spectrum was registered with 128 scans, a 2 s waiting time between scans ($d_1$) and a 1 s FID detection time.

Diffusion-ordered spectroscopy (DOSY) spectra were acquired for each sample using the PE-BPPST-WG1 sequence [92]. For $H_2O$ signal suppression during the final part of the sequence, a soft watergate with a 4 ms selective pulse was used. For the nanocomplex suspension, the bipolar gradients were 1 + 1 ms, and the diffusion time was Δ 300 ms. For control samples consisting of solutions of each component of the nanocarriers at the same concentration, they were in the nanocomplex suspension, the bipolar gradients were 2 + 2 ms, and the diffusion time was Δ 300 ms. The bipolar gradient codifying diffusion was linearly changed between 1 and 47 G/cm to detect 32 points in the diffusion dimension.

WaterLOGSY spectra [93] were acquired by applying a Gaussian selective inversion pulse of 25 ms over the water signal at ~4.7 ppm and a mixing time of 1 s. The spectrum was registered with 128 scans, a 2 s waiting time between scans ($d_1$) and a 1 s FID detection time.

#### 4.2.7. Colloidal stability of the enveloped nanocomplexes in biorelevant media

The colloidal stability of the nanocarriers in simulated intestinal fluid (SIF) was evaluated by analyzing the particle size and PDI by DLS, while the particle concentration in the sample was monitored by the light intensity count rate [44,68]. SIF media (pH 6.8) was produced as described in the pharmacopeia (pH. Eur.), in which the nanocomplex formulation was diluted up to the concentration expected to be attained in in vivo studies, considering animal physiology [94] and a target dose of 50 IU/kg in rodents. Thus, 100 μL of the nanocomplex suspension was diluted in 400 μL of SIF and maintained in an incubator at 37 °C (Heidolph Instruments GmbH & Co. KG, Schwabach, Germany) with a horizontal shaking speed of 300 rpm. At determined time points (0 h, 0.5 h, 1 h, 2 h and 4 h), samples were directly measured using Malvern Zetasizer equipment (NanoZS ZEN 3600, Malvern Instruments, Worcestershire, UK) (Attenuator 10). Each analysis was performed in triplicate for at least three different batches. Assessment of the colloidal stability of the formulation in enzyme-supplemented media as well as in other complex biorelevant media (i.e., FaSSIF-V2, FeSSIF-V2) was unfeasible due to the high signal interference of the complex media components, mainly enzyme and/or surfactants, in the formulation upon measurement using Zetasizer equipment.

#### 4.2.8. In vitro insulin release profile

The insulin release profile of the nanocarriers was evaluated upon incubation in SIF media at 37 °C under horizontal shaking (300 rpm, Heidolph Instruments GmbH & Co. KG, Schwabach, Germany). The dilution rate was in accordance with the expected final insulin concentration to be attained in vivo, for which 200-μL aliquots were diluted with 800 μL of SIF and maintained in an incubator. After 0 h, 0.5 h, 1 h, 2 h and 4 h, the samples were ultracentrifuged (Beckman Coulter, Optima L-90 K, Brea, USA, rotor 70.1Ti, 70,000 rpm (average RCF 336,140 g) for 3 h at 15 °C). In the case of the freeze-dried and reconstituted formulations, the ultracentrifugation time was increased to 4 h due to the presence of trehalose in the sample (2 % *w/v* in the release medium), which delayed nanocomplex precipitation due to the increased density of the media. The obtained supernatants were withdrawn, and the corresponding pellets were dissolved in TFA 0.1 % *v*/v. Both the insulin released (supernatants) and remaining associated insulin with the nanocarriers (pellets) at each time point were analyzed by HPLC as described in the above sections.

#### 4.2.9. In vitro insulin protection against enzymatic degradation

The capacity of the nanocarriers to protect the associated insulin against enzymatic degradation was evaluated by quantifying the amount of undegraded insulin remaining after incubation of the formulation with 1 % w/v pancreatin (4 USP)-supplemented SIF (SIF-p). To this aim and prior to the study, several dilutions of SIF-p and insulin solution in nanocarrier suspension media were mixed and incubated for 20 min (37 °C, 300 rpm horizontal shaking speed), and the reaction was subsequently stopped by adding 0.1 N HCl and placing the mixture on ice. Next, the undegraded insulin was analyzed by HPLC (Section 2.1.3). The pancreatin:insulin ratio at which the half-life time ($t_{1/2}$) of the free protein was ≈20 min was selected for the proteolysis study to comparatively evaluate the $t_{1/2}$ of the associated insulin in the formulation. For the proteolysis evaluation, 250 μL of either nanocarrier suspension, insulin solution at the same concentration and the same dispersing media as the control, or only dispersing media (pancreatin negative control) was mixed with SIF-p following the previously selected pancreatin:insulin ratio and incubated at 37 °C with 300 rpm horizontal shaking (Heidolph Instruments GmbH & Co. KG, Schwabach, Germany). At predetermined intervals (0, 0.5, 1 and 2 h), the enzyme activity was terminated by adding 300 μL of 0.1 M HCl to each aliquot, which also induced nanocomplex disruption by nanocomplex dissociation at an acidic pH and placing the mixture on ice. The remaining amount of insulin was analyzed by HPLC as previously described.

#### 4.2.10. Cell-based insulin bioactivity assay

The insulin bioactivity of the freeze-dried product was tested in cells along with fresh insulin as a positive control. For this purpose, HepG2 cells originating from a human liver carcinoma, a bona-fide insulin target organ, and enriched in human insulin receptor expression (https://www.proteinatlas.org/ENSG00000171105-INSR/cell) were selected for this study.

The HepG2 cell line was obtained from ECACC (UK, distributed by SIGMA). They were authenticated in the laboratory using a combined panel of 16 STR AmpFiSTR NGM Select kit (4,457,889, Applied Biosystems, Germany) including Identifiler Plus Panel V1 (Applied Biosystems) as the read-out pattern. The 16 STR profiles obtained were compared to the EACC and Cellosaurus-Expasy databases (https://www.cellosaurus.org/). Cells were cultured in growth medium (EMEM supplemented with 10 % FBS, 1 % nonessential amino acids, 2 mM L-glutamine, and 1 % penicillin–streptomycin).

For transfection, Viafect and Turbofect were compared by measuring the transfection efficiency of a commercial plasmid preparation of pMAXGFP following the standard recommended protocols. The efficiency was calculated by measuring the number of GFP fluorescent cells with respect to the total number of cells stained with Hoechst 33258. Apoptosis measured as condensed Hoechst+ cells was also measured and discarded for efficiency. Since Viafect led to a > 95 % efficiency while Turbofect led to an efficiency approaching 65 %, all subsequent experiments were performed using Viafect.

MW48 plates (Costar, Thermo NY USA) were precoated with 100 μg/mL Type I collagen solution in PBS (stock solution: 4 mg/mL) and washed three times with PBS. For each assay, 24,000 HepG2 cells/well were seeded on these wells in growth medium and allowed to grow for one full day. The next day, a transfection mix of DNA plasmid (85 ng of promoter+35 ng empty RSV plasmid/well), Viafect transfection reagent (1.5 μL/well) and EMEM (23.5 μL/well) was prepared for all wells, combined and incubated for 20 min. The plasmids employed were pSynSRE-T-luc, containing the −324 to −225 bp fragment of the hamster HMG-CoA synthase promoter containing the SRE elements upstream of the minimal HMG-CoA synthase TATA box (−28 to +39), and pSynSRE-Mut-T-luc bearing four-point mutations in the promoter SRE elements. Insulin has been shown to regulate HMG-CoA synthase expression through these SRE sites in human cells, and its action is eliminated in the mutated promoter [95].

Moreover, the cell medium was replaced by growth medium plus 2

mM metformin to help reduce the basal luciferase expression while the cells were under transfection. Subsequently, 25 μL of the transfection mix was pipetted per well and incubated for 6 h. Next, three washes with warm PBS were performed, and the cells were transferred to deprived medium (growth medium with only 0.5 % *v*/v FBS), including either an insulin control solution or extracted insulin from the reconstituted freeze-dried nanocomplexes. Insulin extraction was accomplished by acidification of the reconstituted nanocomplexes to induce dissociation (pH 3.5), and this solution was further diluted in PBS at a pH of 7.2 to a final concentration of 4 μIU/mL to yield nonharmful conditions for cell culture. Samples were added to cell wells at 50–500 microIU/mL or equivalent vehicle volume. Each condition was tested with six to eight replicates. After 20 h, the wells were washed three times with PBS, followed by the addition of 40 μL PassiveLysis Buffer/well and incubation for 20 min. The lysates were collected and frozen at −20 °C. Luciferase activity was assayed as described elsewhere [96], using 15 μL of lysate and a Mithras microplate reader (LB940, Berthold, Bad Wildbad Germany). Experiments were performed in triplicate.

Statistics were calculated with GraphPad 7 by first applying a Kolmogorov–Smirnov normality test and second, being normally distributed, an unpaired *t*-test to assess significance. Insulin–vehicle concentrations were plotted in parallel graphics to compare the normal SynSRE-T-luc and the mutated SynSRE-Mut-T-luc promoter.

#### 4.2.11. *In vivo biodistribution of radiolabeled enveloped insulin-Zn nanocomplexes*

The in vivo biodistribution of the enveloped nanocomplexes was investigated by radiolabeling the formulation followed by oral administration to rats and SPECT/CT imaging of the animals, as previously reported [59]. Prior to the study, the radioisotope stability and lack of release in SGF were assayed. The formulation pH and ionic force were adjusted by PBS addition to increase the formulation stability in SGF media. The radiolabeling was performed with Technetium-99 m obtained from a 99Mo-99mTc generator by the stannous chloride method by the formation of ionic-coordination bonds with the hydroxylic (—OH) groups of PEG on the surface of the enveloped nanocomplexes, following a previously described procedure [59]. The process involved a previous step of concentration from 0.64 mg/mL to a final insulin concentration of 1.71 mg/mL to ensure a final formulation concentration suitable for oral dosage after labeling. This was accomplished with ultrafiltration devices (Amicon Ultra 30KDa, with Ultracel® low-binding regenerated cellulose membrane), centrifuging at 5000 g and RT for 2 min (Mikro® 20, Hettich®, Hettich Lab Technology, Tuttlingen, Germany) with mild pipetting in between to prevent aggregation and membrane adsorption, allowing the control of the particle size (NanoS90 equipment, Malvern Instruments, Worcestershire, UK). For the radiolabeling of nanocarriers, a previously described protocol was adapted [61]: 750 μL of concentrated formulation was mixed with 40 μL of an acidified 0.5 mg/mL $SnCl_2$ solution (2 mM HCl in Romil-SpS water), for the later reduction of technetium species, in a closed vial that was subsequently purged with helium for 5 min to minimize oxygen content and avoid the oxidation of prereduced tin. Next, 210 μL $^{99m}TcO_4$ eluent generator in 0.9 % *w/v* NaCl was added to the vial, and the mixture was allowed to react for 30 min at RT. Then, the vial was opened, and the quality control of the labeling was performed by radio-thin layer chromatography (ITCL). For this purpose, 2 μL of the obtained sample was placed over a Whatman 3MM strip (1 × 15 cm) and successively developed with 0.9 % w/v NaCl up to 14 cm, and the radiochemical purity was determined using a MiniGita radiochromatographic system (Raytest GmbH, Dortmund, Germany). The radiochemical purity of the radiolabeled nanocomplexes was 97.2 % (SI).

Male Wistar rats (250 g) were housed and cared for under standard conditions with free access to water and food. All procedures were performed following previously approved protocols by the Ethical and Biosafety Committee guidelines from the University of Navarra. Prior to administration, the animals ($n$ = 4) were fasted for 12 h, and each individual dose of the final radiolabeled formulation (260 μL) was mixed with 70 μL of PBS 22.5 mM to ensure stability through stomach passage. Each animal was dosed by oral gavage with 330 μL of either the final radiolabeled formulation (equivalent to 50 IU/kg insulin dose) or free technetium as a control, with both doses equivalent to 250 μCi per rat (activimeter ATOMLAB 500, Biodex®, Shirley NY, USA). The animals were then anesthetized with 2 % isoflurane gas (flow of oxygen of 0.2 L/min) and imaged using SPECT-CT equipment (Symbia, Siemens Medical System, USA) at 1, 2, 4, 6, 8 and 24 h.

#### 4.2.12. *In vivo efficacy studies on normoglycemic and diabetic rats*

Male Sprague–Dawley rats (250–300 g) were obtained from the Central Animal House, University of Santiago de Compostela (Spain). They were kept under 12 h light/12 h dark cycles and fed a standard laboratory rodent diet (Panlab A04, Panlab laboratories). All animal experiments were reviewed and approved by the ethics committee of the University of Santiago de Compostela (ref. 1500AE/12/FUN01/FIS02/CDG3) according to the European and Spanish regulations for the use of animals in animal studies and were therefore performed in compliance with Directive 2010/63/EU of the European Parliament and Council.

For the in vivo testing of the insulin bioactivity of the formulation after processing, both freshly prepared and freeze-dried formulations were administered subcutaneously (s.c.) to fasted (4 h) healthy rats (n = 4) along with an insulin saline solution as a control [44]. Before administration (0 h), blood samples were withdrawn from the tail vein, and initial blood glucose levels were measured with a hand-held glucometer (Glucocard™ G + meter, Arkray Factory, Japan) and monitored every hour thereafter.

Subsequently, coated Insulin-Zn nanocomplexes were tested for their efficacy in both nondiabetic and diabetic rats following intestinal administration. In the case of nondiabetic rats, male Sprague–Dawley rats (250 g) underwent surgical implantation of an intestinal catheter with the proximal end of the cannula tunneled subcutaneously to exit at the back of the neck and sutured [44,68]. The animals were allowed to recover for 6 days, monitored for their general state and weighed every day. They were fasted for 4 h with free access to water prior to administration. Before administration (0 h), blood samples were withdrawn from the tail vein, and initial blood glucose levels were measured with a hand-held glucometer (Glucocard™ G + meter, Arkray Factory, Japan). Only animals with an initial glucose level over 70 mg/dL were used for the study.

Next, intestinal injections of either the formulation or a free insulin solution in the same dispersion media at a dose of 50 IU/kg were applied ($n$ = 6). Before administration (0 h), blood samples were withdrawn from the tail vein, and initial blood glucose levels were measured with a hand-held glucometer (Glucocard™ G + meter, Arkray Factory, Japan) and monitored every hour thereafter.

In the case of the in vivo assessment in T1DM rats, male Sprague–Dawley rats were previously diabetized 7 days before the experiment. For this purpose, they were fasted overnight with free access to water, followed by intraperitoneal (i.p.) injection of STZ (60 mg/kg) in sodium citrate buffer (50 mM, pH 4.5), freshly prepared and used immediately [71]. The diabetization procedure was applied a second time in rats showing normoglycemic values (<150 mg/dL) after 48 h. The rats were kept under a standard diet for 7 days with daily monitoring of their general state, weight and blood glucose levels by tail vein sampling. To rats presenting blood glucose values above 500 mg/dL, a s.c. injection of insulin (1 IU/kg) was administered to prevent the death of animals due to hyperglycemia, except for the day before the experiment. Overall, the high variability in glycemia dependent on β-cell deficit and potential recovery of each animal in response to STZ injection [71] led us to start out using 30 diabetized animals to ensure a final population for $n$ = 8 rats per study group with initial glucose values over 250 mg/dL. In addition, an overnight (12*h*) fasting period allowed us to attain glucose initial values in a measurable range (< 599 mg/dL). Finally, the intestinal cannulation process was avoided in this case to minimize the

stress of both surgery and STZ diabetization in the same animals in such a short period of time. Thus, a direct intrajejunal injection was carried out in its place, as specified below.

Prior to the experiment and after the fasting period, basal blood glucose levels were measured by tail vein sampling and glucometer measurement. Animals with initial blood glucose values over 250 mg/dL were considered diabetic and used for the study, while those with levels below 250 mg/mL or over 599 mg/dL (upper measurement limit of the glucometer) were discarded. Next, the animals were anesthetized with 2 % isoflurane gas (flow of oxygen of 0.2 L/min), and an incision was performed in the abdominal cavity to locate the intestine and inject intraintestinally either the formulation or a free insulin solution in the same dispersion media at a dose of 50 IU/kg (n = 8). Next, the animals were sutured and allowed to wake up, and their blood glucose was monitored every hour thereafter. The maximum total anesthesia time per animal was 10 min.

#### 4.2.13. Preliminary chronic immunotoxicity evaluation in mice

*4.2.13.1. Administration protocol.* Chronic immune toxicity was investigated for the nanocarriers and the loaded insulin in mice following OECD 407-2008 guidelines ("OECD GUIDELINES FOR THE TESTING OF CHEMICALS – Repeated Dose 28-Day Oral Toxicity Study in Rodents"). Eight-week-old female BALB/c mice (25 g) obtained from Harlan (San Pietro al Natisone, Italy) were housed and cared for under standard conditions with access to water and food ad libitum, and all animal experiments were approved by the local animal ethics committee at the University of Padova and were executed in accordance with governing Italian law and EU directives and guidelines.

Prior to administration, the formulation was concentrated to allow for a single oral administration of a target dose of 100 mg nanocarrier per animal daily, corresponding to 285 IU/kg, which was ~10- to 100-fold higher than the average therapeutic dose in this model [75,97]. For this purpose, 400 μL (18.29 IU/mL) of the nanocarrier suspension was ultrafiltrated (Amicon Ultra 30 kDa, with Ultracel® low-binding regenerated cellulose membrane, centrifuged at 4000*g* and 15 °C for 3 min) down to a target volume of 150 μL (48.76 IU/mL). Next, 50 μL of 50 mM PBS was added to the concentrated suspension to ensure formulation stability during stomach passage. Prior to the study, the maintained formulation size, colloidal stability and lack of release in SGF for up to 2 h were confirmed.

Eight-week-old female BALB/c mice were placed on a low-manganese diet one week before and during the treatments. The mice were treated once a day for 28 days with nanocarrier formulation at a dose of 100 mg of nanocarrier/kg (corresponding to 285 human insulin IU/kg). An insulin solution (285 IU/kg) and the nanocarrier dispersant were used as negative controls, while a 7-day administration of 3 % *w/v* dextran sulfate sodium (DSS) (supplemented drinking water) was performed to induce gastrointestinal tract inflammation (positive control) [98]. As a further control, a group of mice was immunized subcutaneously with insulin in complete Freund adjuvant. In all cases, at least 3 mice were treated for each considered time point. The mice were monitored daily for their overall aspect and weight during treatment and euthanized when displaying excessive discomfort. Overall, no macroscopic side effects were observed aside from the group treated with DSS as a positive control of inflammation (data not shown).

*4.2.13.2. FACS analysis of splenic cell populations.* At the end of the chronic administration protocols, the mice were euthanized, and their spleens were harvested under sterile conditions. Single-cell suspensions were prepared for staining with the indicated antibodies, and FcR binding sites were blocked. The antibodies used were anti-CD11b PE-Cy7 (clone M1/70, catalog no. 552850), anti-LY6G APC-Cy7 (clone 1A8, catalog no. 560600), anti-CD11c APC (clone HL3, catalog no. 550261), anti-I-A/I-E PerCP-Cy5.5 (clone M5/114.15.2, catalog no. 562363), anti-CD4 APC (clone RM4-5, catalog no. 553051), anti-CD80 FITC (clone 16-10A1, catalog no. 553768) (all from BD), anti-CD8 PerCP-Cy5.5 (clone 53-6.7, catalog no. 45-0081-82), anti-Ly6C eFluor 450 (clone HK1.4, catalog no. 48-5932-82), anti-CD3 FITC (clone 145-2C11, catalog no. 100306), anti-CD86 biotin (clone GL1, catalog no. 13-0862-82), (all from eBioscience), and anti-F4/80 FITC (AbDSerotec Aqua Live/Dead® dye (Invitrogen) to analyze cell viability. Cell populations were identified by FACS analysis with a gating strategy previously reported elsewhere [99].

*4.2.13.3. Mouse intestine processing and cryosection preparation.* The gastrointestinal tract (stomach, small intestine and large intestine) was dissected, washed twice with PBS and fixed in 4 % PFA solution overnight at 4 °C. Different portions of dissected GI tracts (duodenum, small intestine and large intestine) were carefully separated under a dissection microscope and first submerged in sucrose 20 % at 4 °C overnight and then in sucrose 30 % at 4 °C overnight. Samples were washed twice with cold PBS, equilibrated in OCT (10 min) and finally included in OCT by submerging the sample in liquid nitrogen after 10 min exposure to liquid nitrogen vapors. The included intestinal samples were kept at -80 °C until further manipulation. Next, they were further processed by equilibrating them at -20 °C for 1 h inside a cryostat, and then 7-μm cryosections were cut and transferred to positively charged slides. The obtained cryosections were air-dried for 30 min at RT and stored at -20 °C prior to immunofluorescence processing.

*4.2.13.4. Indirect immunofluorescence of macrophages and lymphocytes in intestine cryosections.* Stored cryosections were equilibrated for 30 min at RT and rehydrated with PBS. After enclosing the cryosections with a hydrophobic PAP-pen, they were permeabilized with a 0.2 % Triton X-100 solution in PBS for 15 min and washed five times with PBS (5 min/wash), and endogenous autofluorescence was quenched with 1 mg/mL sodium borohydride in cold PBS (three incubations of 10 min each). After quenching, the cryosections were washed with PBS, saturated with 3 % BSA in PBS for 1 h at RT and incubated with rabbit anti-CD3 and rat anti-CD68 primary antibodies, diluted 1/200 in 1 % BSA in PBS, O/N at 4 °C. Once the incubation with primary antibodies was completed, the cryosections were washed five times (5 min/wash) with PBS and incubated with the respective secondary antibodies (goat anti-rat Alexa 561 and goat anti-rabbit Alexa 633) for 2 h at RT. After 5 washes with PBS (5 min each), the cryosections were incubated with DAPI (1/100 in PBS; 405 nm) for 5 min at RT and finally mounted with antifade mounting medium. The mounted cryosections were kept at 4 °C prior to confocal imaging.

*4.2.13.5. Confocal imaging of immunotoxicity markers.* Confocal images were acquired with a Leica TCS SP5 II microscope using a 20×/0.50 NA dry objective and 40 X/1.25 NA oil immersion objectives. Images were acquired with a resolution of 1024 × 1024 pixels, equivalent to 387.5 × 387.5 μm for the 40× immersion objective and 775 × 775 μm for the 20× dry objective. Autofluorescence (514 nm), DAPI (405 nm), CD68 (561 nm) and CD3 (633 nm) fluorescence were acquired using the same acquisition parameters, using cryoslice autofluorescence at 514 nm as a reference. Bright field acquisition was also performed (496 nm). For each observed field, a z-stack (6 to 7 μm) was performed with a step size between 0.4 and 0.5 μm for 20× magnification and 0.2 and 0.4 μm for 40× magnification. The final images were obtained as the sum of the intensities along the z-axis (maximum projection) of the acquired volume. Image brightness and contrast were further processed using ImageJ® software, maintaining identical settings between images.

#### 4.2.14. In vivo insulin bioactivity studies on normoglucemic rats

In addition to the cell-based evaluation of the preservation of insulin bioactivity, the pharmacological effect of both the freshly prepared formulations and freeze-dried, reconstituted formulations was tested by

s.c. administration to rats along with free insulin for comparison [44]. To this aim, male Sprague Dawley rats (250 g) were fasted for 4 h before the study with free access to water. A solution of free insulin, freshly prepared formulation and previously freeze-dried, reconstituted formulation were administered at a dose of 1 IU/kg. Before administration (0 h), blood samples were withdrawn from the tail vein, and initial blood glucose levels were measured with a hand-held glucometer (Glucocard™ G + meter, Arkray Factory, Japan) and monitored every hour thereafter.

#### 4.2.15. *In vivo efficacy studies in pigs*

In vivo efficacy studies in pigs were conducted on 12- to 14-week-old neutered male domestic pigs (*Sus scrofa domesticus*) (15–20 kg) from the Research Institute of Animal Breeding and Nutrition, Herceghalom, Hungary. They were housed in individual caging (1 m × 2.5 m), fed a standard powder diet for domestic pigs twice a day with access to water ad libitum, and allowed to acclimatize for 1 week prior to the study. The studies were designed in accordance with accepted pharmacological principles to meet the requirements of the principles of Hungarian Act 1998: XXVIII regulating animal protection (latest modified by Act 2011 CLVIII) and Government Decree 40/2013 on animal experiments; EEC Directive 2004/27/EC of the European Parliament and of the Council of March 31, 2004 amending Directive 2001/83/EC on the Community code relating to medical products for human use (Official Journal L-136, 30/04/2004, pp. 34-57). Animal handling and care were conducted according to the Guide for the Care and Use of Laboratory Animals, NRC, 2011 and Directive 2010/63/EU (European Parliament and Council, took full effect on 1 January 2013). Special permission for animal studies under number PEI/001/3948-6/2014 was issued by the Pest County Government Office of Food Safety and Animal Health Directorate. All procedures carried out on animals were approved by the local ethical committee of Semmelweis University.

*4.2.15.1. Surgical procedure.* On the day of instrumentation, animals were preanesthetized intramuscularly with Calypsol/Dexdomitor (2–3/0.2-0.3 mL, based on body weight) injections in the stalls to avoid stress and were transported to the operating room sedated. The anesthesia was maintained using isoflurane inhalation narcosis (2–3 %) with oxygen through a muzzle mask. Animals were allowed to breathe spontaneously. Their respiration was monitored using a pulse-oximeter (fixed on the tail), measuring the blood oxygen saturation (SpO2), and their temperature was measured rectally (both parameters were monitored by InnoCare-T Anesthesia Monitor - Innomed Medical Co. Hungary). A capnograph was connected to the muzzle mask to monitor etCO2 (% of end-tidal CO2) and the respiratory rate (CAP10 Medlab, Medlab Medizinische Diagnosegerate GmbH, Karlsruhe, Germany) during the operation.

The pigs were instrumented with a central venous single-lumen catheter set (BBraun Certofix Mono V330, 5 Fr, 30 cm, 16G, Cat. 4,160,290 N) introduced into the *vena cava cranialis* through the *vena maxillaris externa* ➔ *vena jugularis externa*. The catheters' tails with sampling ports were led out subcutaneously through the back, followed by fixation at the exit sites with sutures. All incision areas were shaved and disinfected by liberal application of povidone-iodine 10 % prior to the operation and closed after the fixation of cannulas. The cannulas were washed daily with heparin-saline during the recuperation period. Following the operation, the pigs were transported back to the stalls and observed until spontaneous awakening. Preventive antibiotic treatment (Syvaquinol at a dose of 2.5 mg/kg body weight) and analgesia (rheumocam at a dose of 0.4 mg/kg body weight) were applied.

*4.2.15.2. Formulation administration and sampling.* Prior to formulation administration, the pigs were fasted overnight prior to per os administration of the enteric capsules with a plunger applicator. Before and following administration, pre- (0', control) and posttreatment whole blood samples were collected at predetermined intervals for blood cell and blood glucose analysis, and K3EDTA plasma samples were collected for insulin analysis. Convulsions and hypoglycemic shock signs 6 h after administration in response to the unexpectedly intense effect of the formulations were treated by i.v. injections of 10 % *w/v* glucose. The animals were further monitored until their glycemic profiles stabilized.

K3EDTA samples were centrifuged immediately after collection (1500*g*, 10 min at 4 °C), aliquoted, frozen at −20 °C and subsequently transferred to −80 °C for storage until analysis. Whole blood samples were analyzed immediately by a Diatron Vet hematology analyzer (Diatron MI PLC, Budapest, Hungary) for the following parameters: white blood cells (WBC), red blood cells (RBC), hemoglobin (Hgb), platelets (PLT), lymphocytes (Ly) and granulocytes (Gr). After completion of the study, the pigs were euthanized by i.v. administration of Euthasol (1 mL/10 kg body weight) followed by i.v. injection of cc. KCl solution (15 mL/10 kg body weight). Euthanasia was confirmed before disposing the carcass by observing that there was no respiratory movement for at least 3 min and that the heartbeat had ceased.

*4.2.15.3. Pharmacokinetic evaluation by LC–MS.* The insulin content in the plasma samples obtained from the pig studies was analyzed by liquid chromatography/tandem mass spectrometry (LC/MS) following a sample extraction and analysis methodology described elsewhere [100] with some modifications. Stock solutions of bovine insulin (internal standard, IS) and human insulin for the construction of calibration curves were initially prepared in HCl 0.01 N at 5 mg/mL and subsequently diluted in a freshly prepared premixed solvent of ultrapure water/methanol (80/20) with 0.1 % *v*/v acetic acid. Plasma samples of 250 μL were added to 25 μL of 500 ppb IS stock solution; 0–25 μL human insulin stock solutions (25 ppb and 100 ppb) were used when applicable for the construction of calibration curves; and up to 100 μL of the said solvent was used for a constant final volume of 350 μL in all samples. Next, 750 μL of an acetonitrile–methanol mixture (1:1 *v*/v) was added to each sample as a precipitant. The samples were vortexed and maintained under stirring in an incubator (Heidolph Instruments GmbH & Co. KG, Schwabach, Germany) for 10 min (37 °C, 600 rpm) and then centrifuged (21,000 rcf, 15 °C, 10 min, Eppendorf Centrifuge 5430 R, Eppendorf Ibérica S.L.U., Madrid, Spain). The obtained supernatant was filtered through 0.22 μm PVDF hydrophilic filters (4 mm, SLGVR04NL, Merck Millipore, Germany) and vacuumed at 37 °C until completely evaporated with the aid of a SpeedVac. Finally, the dry samples were reconstituted with 90 μL of a freshly prepared premixed solvent of ultrapure water/methanol (80/20) with 0.1 % v/v acetic acid and subsequently analyzed. All solvents employed were of LC/MS grade with the exception of acetic acid, which was USP, pH. Eur. reagent grade, and low-binding materials and recipients were used at all times.

The UPLC system consisted of an Acquity UPLC® H-class system (Waters Corp, Milford, USA) and a column compartment (Acquity UPLC® CSH™ C18 (2.1 × 50 mm, 1.7 μm; Part number 186005296, Serial no. 01463731715175, Cienytech, Santiago de Compostela, Spain). The experimental analytical conditions were as follows: the mobile phase consisted of 0.1 % formic acid aqueous solution (A) and 0.1 % formic acid acetonitrile solution (B). A gradient program was used as follows: 80 % to 63 % A from 0 to 3.8 min; 63 % to 2 % A from 3.8 to 3.9 min; 2 % A maintained from 3.9 to 4.9 min; 2 % to 80 % A from 5.9 to 5 min, and kept constant up to 7 min to allow the system to equilibrate. The total run time was 7 min. The column temperature was maintained at 40 °C, and the autosampler was thermostatized at 10 °C. The injected volume was 50 μL. Under these conditions, human insulin was eluted at 3.34 ± 0.02 min, and bovine insulin was employed as an internal standard at 3.19 ± 0.02 min. The UPLC system was coupled to a Xevo® Triple Quadrupole Detector (TQD) (Waters Corp, Milford, USA) with an electrospray ionization (ESI) interface. A temperature of 525 °C was selected as the source temperature, and 60 °C was selected as the desolvation temperature. The capillary voltage was 2.0 kV, and the cone

voltage and collision energy were set at 50 V and 3 V, respectively. Nitrogen was used for desolvation and as the cone gas at flow rates of 1000 L/h and 80 L/h, respectively. Argon was used as the collision gas. Mass spectrometric detection was operated in positive mode and set up for multiple reaction monitoring (MRM) to monitor the human insulin transitions of *m/z* 969.0 >> 1133.0 (cone voltage 50 V, collision energy 25 V); 1162.6 >> 143.2 (cone voltage 60 V, collision energy 40 V); 1162.6 >> 219.0 (cone voltage 60 V, collision energy 50 V); 1162.6 >> 226.0 (cone voltage 60 V, collision energy 40 V), and bovine insulin transitions of m/z 956.5 >> 1114.8 (cone voltage 50 V, collision energy 18 V); 956.6 >> 315.2 (cone voltage 50 V, collision energy 50 V); 956.6 >> 1121.2 (cone voltage 50 V, collision energy 18 V); and 1147.5 >> 315.5 (cone voltage 70 V, collision energy 52 V). Calibration curves were constructed over a range of 0.25–5 ppb, with an LOQ of 0.5 ppb. Data acquisition and analysis were performed using TargetLynx v4.1 software (Waters Corp., Milford, USA).

#### *4.2.16. Production and physicochemical characterization of biometal–tRNA nanocomplexes*

Nanocomplexes of tRNA-Zn were prepared by adding a 20 mg/mL zinc acetate dihydrate aqueous solution over 500 μL of a 0.1 mg/mL tRNA solution in HCl 0.01 N to attain a charge ratio (Zn mol–nucleotide) of either 5:1 or 10:1. The mixture was maintained under magnetic stirring at 300 rpm while 0.1 N NaOH was added to adjust the pH to 7.4. Next, the mixture was incubated at 4 °C for 3 h. Subsequently, the mixture was allowed to temper at RT for 4 min, vortexed for 10 s and then characterized in terms of particle size and ZP.

Regarding the tRNA–Fe nanocomplex production, two types of nanocomplexes were produced, namely, Type I nanocomplexes, exhibiting a negative surface charge and ability to be coated with a positively charged material, and Type II nanocomplexes, exhibiting a positive surface charge and ability to be coated with a negatively charged material. To produce Type I nanocomplexes, a 0.1 mg/mL tRNA solution in RNAse-free water and a 0.246 mg/mL ferric chloride hexahydrate solution in acetate buffer (100 mM) (pH 6) were prepared. Next, the ferric chloride hexahydrate solution was added dropwise over the tRNA solution under stirring (500 rpm) at a 1:1 *v*/v ratio, and the mixture was stirred for 10 min. To coat the resulting nanocomplexes, the obtained suspension was immediately added dropwise over a 0.1 mg/mL solution of the selected positively charged polymer (chitosan or polyarginine (PARG)) under stirring (500 rpm) at a 1:1 v/v ratio, and the mixture was stirred for 10 min. To produce Type II nanocomplexes, a 0.1 mg/mL tRNA solution in RNAse-free water and a 2.216 mg/mL ferric chloride hexahydrate solution in acetate buffer (100 mM) (pH 6) were prepared. Next, the tRNA solution was added dropwise over the ferric chloride hexahydrate solution under stirring (500 rpm) at a 1:1 v/v ratio, and the mixture was stirred for 10 min. To coat the resulting nanocomplexes, the obtained suspension was immediately added dropwise over a 2 mg/mL solution of the selected negatively charged polymer ((HA), CS, PEG(5 k)-PGA(10) or PSA) under stirring (500 rpm) at a 1:1 v/v ratio, and the mixture was stirred for 10 min.

The particle size distribution and PDI were determined by DLS, and the ZP was determined from the electrophoretic mobility values obtained by LDA using Malvern Zetasizer equipment (NanoZS ZEN 3600, Malvern Instruments, Worcestershire, UK) equipped with a red laser light beam ($\lambda = 632.8$ nm). The formulations were directly measured without dilution at 25 °C with at least three different batches and triplicate analysis of each batch.

#### *4.2.17. Statistics*

All experiments were performed at least in triplicate, and data are presented as the means ± standard deviations (SDs) in physicochemical studies and the standard errors of the mean (SEMs) for in vivo studies. Statistical analysis was carried out using one-way analysis of variance (ANOVA) with a multiple comparisons test (GraphPad Prism, GraphPad software Inc., CA, USA). All other analyses were performed using one-way analysis of variance (ANOVA). The level of significance was set at probabilities of $^{*}p < 0.05$, $^{**}p < 0.01$, $^{***}p < 0.001$ and $^{****}$ $p < 0.0001$.


## Funding statement

This work was supported by the European TRANS-INT Consortium, which received funding from the European Union's Seventh Framework Programme for research, technological development and demonstration under grant agreement NO. 281035. M. Durán-Lobato acknowledges a postdoctoral fellowship (Contrato de Acceso al Sistema Español de Ciencia, Tecnología e Innovación (grant number USE-19533-Y)) granted by "VI Plan Propio" from the University of Seville.


## CRediT authorship contribution statement

**Matilde Durán-Lobato:** Writing – review & editing, Writing – original draft, Visualization, Validation, Methodology, Investigation, Formal analysis, Data curation, Conceptualization. **Sulay Tovar:** Writing – review & editing, Supervision, Resources, Project administration, Methodology, Investigation, Funding acquisition, Formal analysis, Conceptualization. **Juan Cuñarro:** Validation, Investigation, Formal analysis, Data curation. **Rocío Ramos-Membrive:** Validation, Investigation, Formal analysis, Data curation. **Iván Peñuelas:** Writing – review & editing, Supervision, Resources, Methodology, Investigation, Funding acquisition, Conceptualization. **Ilaria Marigo:** Writing – review & editing, Validation, Supervision, Resources, Project administration, Methodology, Investigation, Funding acquisition, Formal analysis, Data curation, Conceptualization. **Federico Benetti:** Writing – review & editing, Validation, Resources, Methodology, Investigation, Funding acquisition, Formal analysis, Data curation, Conceptualization. **Miguel Chenlo:** Validation, Supervision, Resources, Methodology, Formal analysis, Data curation. **Clara V. Álvarez:** Writing – review & editing, Supervision, Resources, Methodology, Funding acquisition, Conceptualization. **Vashegyi Ildikó:** Validation, Investigation, Formal analysis, Data curation, Conceptualization. **Rudolf Urbanics:** Validation, Supervision, Methodology, Investigation, Formal analysis, Data curation, Conceptualization. **János Szebeni:** Writing – review & editing, Supervision, Resources, Funding acquisition, Conceptualization. **María José Alonso:** Writing – review & editing, Supervision, Resources, Funding acquisition, Conceptualization.

## Declaration of competing interest

The authors declare that they have no known competing financial interests or personal relationships that could have appeared to influence the work reported in this paper.

## Data availability

Data will be made available on request.


## Acknowledgments

The authors are especially grateful for Dr. Álvaro Antelo for his assistance with LC–MS method development and analysis, Dr. Manuel Martín-Pastor (Nuclear Magnetic Resonance Unit, RIADT, Universidade de Santiago de Compostela) for his assistance with NMR experimental design and interpretation, Dr. Bruno Dacuña Mariño for his help with Rx experimental design and interpretation (X-ray Unit, Crystalline Powder Section, RIAIDT, Universidade de Santiago de Compostela, Maria Suarez-Fariña for the technical help with cell-based bioactivity assays, and Sanofi for providing the human insulin peptide as well as assistance with peptide handling and analysis.

## Appendix A. Supplementary data

Supplementary data to this article can be found online at https://doi.org/10.1016/j.jconrel.2024.11.016.

## References


[1] A.N. Zelikin, C. Ehrhardt, A.M. Healy, Materials and methods for delivery of biological drugs, Nat. Chem. 8 (2016) 997–1007, https://doi.org/10.1038/nchem.2629.

[2] J. Byrne, H.W. Huang, J.C. McRae, S. Babaee, A. Soltani, S.L. Becker, G. Traverso, Devices for drug delivery in the gastrointestinal tract: a review of systems physically interacting with the mucosa for enhanced delivery, Adv. Drug Deliv. Rev. 177 (2021) 113926, https://doi.org/10.1016/j.addr.2021.113926.

[3] T.D. Brown, K.A. Whitehead, S. Mitragotri, Materials for oral delivery of proteins and peptides, Nat. Rev. Mater. 5 (2020) 127–148, https://doi.org/10.1038/s41578-019-0156-6.

[4] A.C. Anselmo, Y. Gokarn, S. Mitragotri, Non-invasive delivery strategies for biologics, Nat. Rev. Drug Discov. 18 (2018) 19–40, https://doi.org/10.1038/nrd.2018.183.

[5] M. Durán-Lobato, A.M. López-Estévez, A.S. Cordeiro, T.G. Dacoba, J. Crecente-Campo, D. Torres, M.J. Alonso, Nanotechnologies for the delivery of biologicals: historical perspective and current landscape, Adv. Drug Deliv. Rev. 176 (2021), https://doi.org/10.1016/j.addr.2021.113899.

[6] D.J. Brayden, T.A. Hill, D.P. Fairlie, S. Maher, R.J. Mrsny, Systemic delivery of peptides by the oral route: formulation and medicinal chemistry approaches, Adv. Drug Deliv. Rev. (2020), https://doi.org/10.1016/j.addr.2020.05.007.

[7] M. Durán-Lobato, Z. Niu, M.J. Alonso, Oral delivery of biologics for precision medicine, Adv. Mater. 32 (2019), https://doi.org/10.1002/adma.201901935.

[8] A. Banerjee, K. Ibsen, T. Brown, R. Chen, C. Agatemor, S. Mitragotri, Ionic liquids for oral insulin delivery, Proc. Natl. Acad. Sci. 115 (2018) 7296–7301, https://doi.org/10.1073/pnas.1722338115.

[9] A. Banerjee, R. Chen, S. Arafin, S. Mitragotri, Intestinal iontophoresis from mucoadhesive patches: a strategy for oral delivery, J. Control. Release 297 (2019) 71–78, https://doi.org/10.1016/j.jconrel.2019.01.037.

[10] A. Abramson, E. Caffarel-Salvador, M. Khang, D. Dellal, D. Silverstein, Y. Gao, M. R. Frederiksen, A. Vegge, F. Hubalek, J.J. Water, A.V. Friederichses, J. Fels, R. K. Kirk, C. Cleveland, J. Collins, S. Tamang, A. Hayward, T. Landh, S.T. Buckley, N. Roxhed, U. Rahbek, R. Langer, G. Traverso, An ingestible self-orienting applicator for oral delivery of macromolecules, Sci. (Under Rev.) 363 (2019) 611–615, https://doi.org/10.1126/SCIENCE.AAU2277.

[11] A. Abramson, E. Caffarel-Salvador, V. Soares, D. Minahan, R.Y. Tian, X. Lu, D. Dellal, Y. Gao, S. Kim, J. Wainer, J. Collins, S. Tamang, A. Hayward, T. Yoshitake, H.C. Lee, J. Fujimoto, J. Fels, M.R. Frederiksen, U. Rahbek, N. Roxhed, R. Langer, G. Traverso, A luminal unfolding microneedle injector for oral delivery of macromolecules, Nat. Med. 25 (2019) 1512–1518, https://doi.org/10.1038/s41591-019-0598-9.

[12] A. Abramson, M.R. Frederiksen, A. Vegge, B. Jensen, M. Poulsen, B. Mouridsen, M.O. Jespersen, R.K. Kirk, J. Windum, F. Hubálek, J.J. Water, J. Fels, S. B. Gunnarsson, A. Bohr, E.M. Straarup, M.W.H. Ley, X. Lu, J. Wainer, J. Collins, S. Tamang, K. Ishida, A. Hayward, P. Herskind, S.T. Buckley, N. Roxhed, R. Langer, U. Rahbek, G. Traverso, Oral delivery of systemic monoclonal antibodies, peptides and small molecules using gastric auto-injectors, Nat. Biotechnol. 40 (2022) 103–109, https://doi.org/10.1038/s41587-021-01024-0.

[13] M. Hashim, R. Korupolu, B. Syed, K. Horlen, S. Beraki, P. Karamchedu, A. K. Dhalla, R. Ruffy, M. Imran, Jejunal wall delivery of insulin via an ingestible capsule in anesthetized swine—a pharmacokinetic and pharmacodynamic study, Pharmacol. Res. Perspect. 7 (2019) 1–6, https://doi.org/10.1002/prp2.522.

[14] W. Chen, J. Wainer, S.W. Ryoo, X. Qi, R. Chang, J. Li, S.H. Lee, S. Min, A. Wentworth, J.E. Collins, S. Tamang, K. Ishida, A. Hayward, R. Langer, G. Traverso, Dynamic omnidirectional adhesive microneedle system for oral macromolecular drug delivery, Sci. Adv. 8 (2022) 1–11, https://doi.org/10.1126/sciadv.abk1792.

[15] S.T. Buckley, T.A. Bækdal, A. Vegge, S.J. Maarbjerg, C. Pyke, J. Ahnfelt-Rønne, K. G. Madsen, S.G. Schéele, T. Alanentalo, R.K. Kirk, B.L. Pedersen, R. B. Skyggebjerg, A.J. Benie, H.M. Strauss, P.O. Wahlund, S. Bjerregaard, E. Farkas, C. Fekete, F.L. Søndergaard, J. Borregaard, M.L. Hartoft-Nielsen, L.B. Knudsen, Transcellular stomach absorption of a derivatized glucagon-like peptide-1 receptor agonist, Sci. Transl. Med. 10 (2018), https://doi.org/10.1126/scitranslmed.aar7047.

[16] D.J. Brayden, S. Maher, Transient permeation enhancer® (TPE®) technology for oral delivery of octreotide: a technological evaluation, Expert Opin. Drug Deliv. 18 (2021) 1501–1512, https://doi.org/10.1080/17425247.2021.1942838.

[17] E. Caffarel-Salvador, A. Abramson, R. Langer, G. Traverso, Oral delivery of biologics using drug-device combinations, Curr. Opin. Pharmacol. 36 (2017) 8–13, https://doi.org/10.1016/j.coph.2017.07.003.

[18] T.V. O'Halloran, M. Kebede, S.J. Philips, A.D. Attie, Zinc, insulin, and the liver: a ménage à trois, J. Clin. Invest. 123 (2013) 4136–4139, https://doi.org/10.1172/JCI72325.

[19] J.J. Abel, Crystalline Insulin, Proc. Natl. Acad. Sci. USA 12 (1926) 132–136, https://doi.org/10.1073/pnas.12.2.132.

[20] K. Hallas-Møller, K. Petersen, J. Schlichtkrull, Crystalline and amorphous insulin-zinc compounds with prolonged action, Science 116 (1952) 394–398, https://doi.org/10.1126/science.116.3015.394.

[21] G.P. Carino, J.S. Jacob, E. Mathiowitz, Nanosphere based oral insulin delivery, J. Control. Release 65 (2000) 261–269, https://doi.org/10.1016/S0168-3659(99)00247-3.

[22] X. Han, Y. Lu, J. Xie, E. Zhang, H. Zhu, H. Du, K. Wang, B. Song, C. Yang, Y. Shi, Z. Cao, Zwitterionic micelles efficiently deliver oral insulin without opening tight junctions, Nat. Nanotechnol. 15 (2020) 605–614, https://doi.org/10.1038/s41565-020-0693-6.

[23] D. Hristov, F. McCartney, J. Beirne, E. Mahon, S. Reid, S. Bhattacharjee, G. Penarier, U. Werner, D. Bazile, D.J. Brayden, Silica-coated nanoparticles with a Core of zinc, l -arginine, and a peptide designed for Oral delivery, ACS Appl. Mater. Interfaces 12 (2020) 1257–1269, https://doi.org/10.1021/acsami.9b16104.

[24] M.F. Dunn, Zinc-ligand interactions modulate assembly and stability of the insulin hexamer - a review, in, BioMetals (2005) 295–303, https://doi.org/10.1007/s10534-005-3685-y.

[25] Y.V. Li, Zinc and insulin in pancreatic beta-cells, Endocrine 45 (2014) 178–189, https://doi.org/10.1007/s12020-013-0032-x.

[26] X. Han, Y. Lu, J. Xie, E. Zhang, H. Zhu, H. Du, K. Wang, B. Song, C. Yang, Y. Shi, Z. Cao, Zwitterionic micelles efficiently deliver oral insulin without opening tight junctions, Nat. Nanotechnol. 15 (2020) 605–614, https://doi.org/10.1038/s41565-020-0693-6.

[27] A. Banerjee, J. Qi, R. Gogoi, J. Wong, S. Mitragotri, Role of nanoparticle size, shape and surface chemistry in oral drug delivery, J. Control. Release 238 (2016) 176–185, https://doi.org/10.1016/j.jconrel.2016.07.051.

[28] K. Nadendla, S.H. Friedman, Light Control of Protein Solubility Through Isoelectric Point Modulation, 2017, https://doi.org/10.1021/jacs.7b08465.

[29] M. Weiss, Design of ultra-stable insulin analogues for the developing world, J. Health Specialties 1 (2013) 59, https://doi.org/10.4103/1658-600X.114683.

[30] T.L. Blundell, J.F. Cutfield, S.M. Cutfield, E.J. Dodson, G.G. Dodson, D. C. Hodgkin, D.A. Mercola, M. Vijayan, Atomic positions in rhombohedral 2-zinc insulin crystals, Nature 231 (1971) 506–511, https://doi.org/10.1038/231506a0.

[31] P.J. Wyatt, Measurement of special nanoparticle structures by light scattering, Anal. Chem. 86 (2014) 7171–7183, https://doi.org/10.1021/ac500185w.

[32] A. Banerjee, J. Qi, R. Gogoi, J. Wong, S. Mitragotri, Role of nanoparticle size, shape and surface chemistry in oral drug delivery, J. Control. Release 238 (2016) 176–185, https://doi.org/10.1016/j.jconrel.2016.07.051.

[33] D. Li, J. Zhuang, H. He, S. Jiang, A. Banerjee, Y. Lu, W. Wu, S. Mitragotri, L. Gan, J. Qi, Influence of particle geometry on gastrointestinal transit and absorption following Oral administration, ACS Appl. Mater. Interfaces 9 (2017) 42492–42502, https://doi.org/10.1021/acsami.7b11821.

[34] M. Guo, M. Wei, W. Li, M. Guo, C. Guo, M. Ma, Y. Wang, Z. Yang, M. Li, Q. Fu, L. Yang, Z. He, Impacts of particle shapes on the oral delivery of drug nanocrystals: mucus permeation, transepithelial transport and bioavailability, J. Control. Release 307 (2019) 64–75, https://doi.org/10.1016/j.jconrel.2019.06.015.

[35] R. Gupta, Y. Badhe, S. Mitragotri, B. Rai, Permeation of nanoparticles across the intestinal lipid membrane: dependence on shape and surface chemistry studied through molecular simulations, Nanoscale 12 (2020) 6318–6333, https://doi.org/10.1039/c9nr09947f.

[36] C. Bao, B. Liu, B. Li, J. Chai, L. Zhang, L. Jiao, D. Li, Z. Yu, F. Ren, X. Shi, Y. Li, Enhanced transport of shape and rigidity-tuned α-Lactalbumin nanotubes across intestinal mucus and cellular barriers, Nano Lett. 20 (2020) 1352–1361, https://doi.org/10.1021/acs.nanolett.9b04841.

[37] C. Manoharan, J. Singh, Insulin loaded PLGA microspheres: effect of zinc salts on encapsulation, release, and stability, J. Pharm. Sci. 98 (2009) 529–542, https://doi.org/10.1002/jps.21445.

[38] Q. Xu, L.M. Ensign, N.J. Boylan, A. Schön, X. Gong, J.C. Yang, N.W. Lamb, S. Cai, T. Yu, E. Freire, J. Hanes, Impact of surface polyethylene glycol (PEG) density on biodegradable nanoparticle transport in mucus ex vivo and distribution in vivo, ACS Nano 9 (2015) 9217–9227, https://doi.org/10.1021/acsnano.5b03876.

[39] A. Vila, A. Sánchez, M. Tobío, P. Calvo, M.J. Alonso, Design of biodegradable particles for protein delivery, J. Control. Release 78 (2002) 15–24, https://doi.org/10.1016/S0168-3659(01)00486-2.

[40] S. Maher, R.J. Mrsny, D.J. Brayden, Intestinal permeation enhancers for oral peptide delivery, Adv. Drug Deliv. Rev. 106 (2016) 277–319, https://doi.org/10.1016/j.addr.2016.06.005.

[41] K. Chi, J.M. Catchmark, Crystalline nanocellulose/lauric arginate complexes, Carbohydr. Polym. 175 (2017) 320–329, https://doi.org/10.1016/j.carbpol.2017.08.005.

[42] X. Yang, R. Rai, C.N. Huu, N. Nitin, Synergistic antimicrobial activity by light or thermal treatment and lauric arginate: membrane damage and oxidative stress, Appl. Environ. Microbiol. 85 (2019) 1–14, https://doi.org/10.1128/AEM.01033-19.

[43] A. Pensado, M. Martín-Pastor, G.K. Zorzi, E.S. Carvalho, A. Sanchez, Structural analysis of nanosystems: solid Sorbitan esters nanoparticles (SSN) as a case study, Eur. J. Pharm. Biopharm. 104 (2016) 189–199, https://doi.org/10.1016/j.ejpb.2016.05.002.

[44] Z. Niu, E. Tedesco, F. Benetti, A. Mabondzo, I.M.I.M. Montagner, I. Marigo, D. Gonzalez-Touceda, S. Tovar, C. Diéguez, M.J.M.J. Santander-Ortega, M.J.M. J. Alonso, Rational design of polyarginine nanocapsules intended to help peptides overcoming intestinal barriers, J. Control. Release 263 (2017) 4–17, https://doi.org/10.1016/j.jconrel.2017.02.024.

[45] L.N. Thwala, D.P. Delgado, K. Leone, I. Marigo, F. Benetti, M. Chenlo, C. V. Alvarez, S. Tovar, C. Dieguez, N.S. Csaba, M.J. Alonso, Protamine

nanocapsules as carriers for oral peptide delivery, J. Control. Release 291 (2018) 157–168, https://doi.org/10.1016/j.jconrel.2018.10.022.
[46] T.V. O'Halloran, M. Kebede, S.J. Philips, A.D. Attie, Zinc, insulin, and the liver: a ménage à trois, J. Clin. Invest. 123 (2013) 4136–4139, https://doi.org/10.1172/JCI72325.
[47] R. Pohl, R. Hauser, M. Li, E. De Souza, R. Feldstein, R. Seibert, K. Ozhan, N. Kashyap, S. Steiner, Ultra-rapid absorption of recombinant human insulin induced by zinc chelation and surface charge masking, J. Diabetes Sci. Technol. 6 (2012), https://doi.org/10.1177/193229681200600404.
[48] A.C. Anselmo, S. Mitragotri, Nanoparticles in the clinic, Bioeng. Transl. Med. 1 (2016) 10–29, https://doi.org/10.1002/btm2.10003.
[49] S. Hassan, G. Prakash, A. Bal Ozturk, S. Saghazadeh, M. Farhan Sohail, J. Seo, M. Remzi Dokmeci, Y.S. Zhang, A. Khademhosseini, Evolution and clinical translation of drug delivery nanomaterials, Nano Today 15 (2017) 91–106, https://doi.org/10.1016/j.nantod.2017.06.008.
[50] M. Durán-Lobato, Z. Niu, M.J. Alonso, Oral delivery of biologics for precision medicine, Adv. Mater. 32 (2019), https://doi.org/10.1002/adma.201901935.
[51] E. Presas, F. McCartney, E. Sultan, C. Hunger, S. Nellen, C.V. Alvarez, U. Werner, D. Bazile, D.J. Brayden, C.M. O'Driscoll, Physicochemical, pharmacokinetic and pharmacodynamic analyses of amphiphilic cyclodextrin-based nanoparticles designed to enhance intestinal delivery of insulin, J. Control. Release 286 (2018) 402–414, https://doi.org/10.1016/j.jconrel.2018.07.045.
[52] J. Heade, F. McCartney, M. Chenlo, O.M. Marro, M. Severic, R. Kent, S.B. Bleiel, C.V. Alvarez, B.T. Griffin, D.J. Brayden, Synthesis and in vivo evaluation of insulin-loaded whey beads as an oral peptide delivery system, Pharmaceutics 13 (2021), https://doi.org/10.3390/pharmaceutics13050656.
[53] Y. Zhou, Z. Chen, D. Zhao, D. Li, C. He, X. Chen, A pH-triggered self-unpacking capsule containing Zwitterionic hydrogel-coated MOF nanoparticles for efficient Oral Exendin-4 delivery, Adv. Mater. 33 (2021) 1–10, https://doi.org/10.1002/adma.202102044.
[54] A.M.M. Sadeghi, M.R. Avadi, S. Ejtemaimehr, S. Abashzadeh, A. Partoazar, F. Dorkoosh, M. Faghihi, M. Rafiee-Tehrani, H.E. Junginger, Development of a gas empowered drug delivery system for peptide delivery in the small intestine, J. Control. Release 134 (2009) 11–17, https://doi.org/10.1016/j.jconrel.2008.10.012.
[55] E.Y. Chuang, K.J. Lin, P.Y. Lin, H.L. Chen, S.P. Wey, F.L. Mi, H.C. Hsiao, C. T. Chen, H.W. Sung, Self-assembling bubble carriers for oral protein delivery, Biomaterials 64 (2015) 115–124, https://doi.org/10.1016/j.biomaterials.2015.06.035.
[56] P.Y. Lin, E.Y. Chuang, Y.H. Chiu, H.L. Chen, K.J. Lin, J.H. Juang, C.H. Chiang, F. L. Mi, H.W. Sung, Safety and efficacy of self-assembling bubble carriers stabilized with sodium dodecyl sulfate for oral delivery of therapeutic proteins, J. Control. Release 259 (2017) 168–175, https://doi.org/10.1016/j.jconrel.2016.12.018.
[57] A. Karole, S. Parvez, R.S. Thakur, S.L. Mudavath, Effervescent based nano-gas carrier enhanced the bioavailability of poorly aqueous soluble drug: a comprehensive mechanistic understanding, J. Drug Deliv. Sci. Technol. 69 (2022) 103167, https://doi.org/10.1016/j.jddst.2022.103167.
[58] T.S. Coffey, Diet coke and Mentos: what is really behind this physical reaction? Am. J. Phys. 76 (2008) 551–557, https://doi.org/10.1119/1.2888546.
[59] Z. Niu, E. Samaridou, E. Jaumain, J. Coëne, G. Ullio, N. Shrestha, J. Garcia, M. Durán-Lobato, S. Tovar, M.J. Santander-Ortega, M.V. Lozano, M.M. Arroyo-Jimenez, R. Ramos-Membrive, I. Peñuelas, A. Mabondzo, V. Préat, M. Teixidó, E. Giralt, M.J. Alonso, PEG-PGA enveloped octaarginine-peptide nanocomplexes: an oral peptide delivery strategy, J. Control. Release 276 (2018) 125–139, https://doi.org/10.1016/j.jconrel.2018.03.004.
[60] X. Yu, D. Gao, L. Gao, J. Lai, C. Zhang, Y. Zhao, L. Zhong, B. Jia, F. Wang, X. Chen, Z. Liu, Inhibiting metastasis and preventing tumor relapse by triggering host immunity with tumor-targeted photodynamic therapy using photosensitizer-loaded functional nanographenes, ACS Nano 11 (2017) 10147–10158, https://doi.org/10.1021/acsnano.7b04736.
[61] P. Areses, M.T. Agüeros, G. Quincoces, M. Collantes, J.A. Richter, L. López-Sánchez, M. Sánchez-Martínez, J.M. Irache, I. Peñuelas, Molecular imaging techniques to study the biodistribution of orally administered 99m Tc-labelled naive and ligand-tagged nanoparticles, Mol. Imaging Biol. 13 (2011) 1215–1223, https://doi.org/10.1007/s11307-010-0456-0.
[62] J.M. DeSesso, C.F. Jacobson, Anatomical and physiological parameters affecting gastrointestinal absorption in humans and rats, Food Chem. Toxicol. 39 (2001) 209–228.
[63] M.C. Torjman, J.I. Joseph, C. Munsick, M. Morishita, Z. Grunwald, Effects of isoflurane on gastrointestinal motility after brief exposure in rats, Int. J. Pharm. 294 (2005) 65–71, https://doi.org/10.1016/j.ijpharm.2004.12.028.
[64] N. Dragicevic, H.I. Maibach, Nina Dragicevic, Howard I. Maibach (Eds.), Percutaneous Penetration Enhancers Chemical Methods in Penetration Enhancement_ Modification of the Stratum Corneum (2015), Springer-Verlag, 2015. Berlin Heid.pdf.
[65] J. Jiao, Polyoxyethylated nonionic surfactants and their applications in topical ocular drug delivery, Adv. Drug Deliv. Rev. 60 (2008) 1663–1673, https://doi.org/10.1016/j.addr.2008.09.002.
[66] M. Morishita, T. Goto, N.A. Peppas, J.I. Joseph, M.C. Torjman, C. Munsick, K. Nakamura, T. Yamagata, K. Takayama, A.M. Lowman, Mucosal insulin delivery systems based on complexation polymer hydrogels: effect of particle size on insulin enteral absorption, J. Control. Release 97 (2004) 115–124, https://doi.org/10.1016/j.jconrel.2004.03.008.
[67] M. Morishita, N. Kamei, J. Ehara, K. Isowa, K. Takayama, A novel approach using functional peptides for efficient intestinal absorption of insulin, J. Control. Release 118 (2007) 177–184, https://doi.org/10.1016/j.jconrel.2006.12.022.
[68] L.N. Thwala, A. Beloqui, N.S. Csaba, D. González-Touceda, S. Tovar, C. Dieguez, M.J. Alonso, V. Préat, V.P. Lungile Nomcebo Thwala, Ana Beloqui, Noemi Stefania Csaba, David González-Touceda, Sulay Tovar, Carlos Dieguez, Maria Jose Alonso, The interaction of protamine nanocapsules with the intestinal epithelium: a mechanistic approach, J. Control. Release 243 (2016) 109–120, https://doi.org/10.1016/j.jconrel.2016.10.002.
[69] I. Santalices, C. Vázquez-Vázquez, M.J. Santander-Ortega, V. Lozano, F. Araújo, B. Sarmento, N. Shrestha, V. Préat, M. Chenlo, C.V. Alvarez, F. Benetti, J. Cuñarro, S. Tovar, D. Torres, M.J. Alonso, A nanoemulsion/micelles mixed nanosystem for the oral administration of hydrophobically modified insulin, Drug Deliv. Transl. Res. 11 (2021) 524–545, https://doi.org/10.1007/s13346-021-00920-x.
[70] C. Damge, C. Michel, M. Aprahamian, P. Couvreur, New approach for oral administration of insulin with polyalkylcyanoacrylate nanocapsules as drug carrier, Diabetes 37 (1988) 246–251, https://doi.org/10.2337/diab.37.2.246.
[71] B.L. Furman, Streptozotocin-induced diabetic models in mice and rats, Curr. Protoc. Pharmacol. 70 (2015) 5.47.1–5.47.20, https://doi.org/10.1002/0471141755.ph0547s70.
[72] A. Viehof, L. Javot, A. Béduneau, Y. Pellequer, A. Lamprecht, Oral insulin delivery in rats by nanoparticles prepared with non-toxic solvents, Int. J. Pharm. 443 (2013) 169–174, https://doi.org/10.1016/j.ijpharm.2013.01.017.
[73] A. Makhlof, Y. Tozuka, H. Takeuchi, Design and evaluation of novel pH-sensitive chitosan nanoparticles for oral insulin delivery, Eur. J. Pharm. Sci. 42 (2011) 445–451, https://doi.org/10.1016/j.ejps.2010.12.007.
[74] C. Damgé, C. Michel, M. Aprahamian, P. Couvreur, J.P. Devissaguet, Nanocapsules as carriers for oral peptide delivery, J. Control. Release 13 (1990) 233–239, https://doi.org/10.1016/0168-3659(90)90013-J.
[75] E.M. Pridgen, F. Alexis, T.T. Kuo, E. Levy-Nissenbaum, R. Karnik, R.S. Blumberg, R. Langer, O.C. Farokhzad, Transepithelial transport of fc-targeted nanoparticles by the neonatal fc receptor for oral delivery, Sci. Transl. Med. 5 (2013), https://doi.org/10.1126/scitranslmed.3007049.
[76] W. Shan, X. Zhu, M. Liu, L. Li, J. Zhong, W. Sun, Z. Zhang, Y. Huang, Overcoming the diffusion barrier of mucus and absorption barrier of epithelium by self-assembled nanoparticles for oral delivery of insulin, ACS Nano 9 (2015) 2345–2356, https://doi.org/10.1021/acsnano.5b00028.
[77] M. Morishita, T. Goto, K. Nakamura, A.M. Lowman, K. Takayama, N.A. Peppas, Novel oral insulin delivery systems based on complexation polymer hydrogels: single and multiple administration studies in type 1 and 2 diabetic rats, J. Control. Release 110 (2006) 587–594, https://doi.org/10.1016/j.jconrel.2005.10.029.
[78] R.L. Jump, A.D. Levine, Mechanisms of natural tolerance in the intestine: implications for inflammatory bowel disease, Inflamm. Bowel Dis. 10 (2004) 462–478, https://doi.org/10.1097/00054725-200407000-00023.
[79] R.V. Overgaard, A. Navarria, S.H. Ingwersen, T.A. Bækdal, R.J. Kildemoes, Clinical pharmacokinetics of Oral Semaglutide: analyses of data from clinical pharmacology trials, Clin. Pharmacokinet. 60 (2021) 1335–1348, https://doi.org/10.1007/s40262-021-01025-x.
[80] P. Tyagi, R. Trivedi, S. Pechenov, C. Patel, J. Revell, S. Wills, Y. Huang, A. I. Rosenbaum, J.A. Subramony, Targeted oral peptide delivery using multi-unit particulates: drug and permeation enhancer layering approach, J. Control. Release 338 (2021) 784–791, https://doi.org/10.1016/j.jconrel.2021.09.002.
[81] S. Bonengel, M. Jelkmann, M. Abdulkarim, M. Gumbleton, V. Reinstadler, H. Oberacher, F. Prüfert, A. Bernkop-Schnürch, Impact of different hydrophobic ion pairs of octreotide on its oral bioavailability in pigs, J. Control. Release 273 (2018) 21–29, https://doi.org/10.1016/j.jconrel.2018.01.012.
[82] S. Berg, J. Krause, A. Björkbom, K. Walter, S. Harun, A. Granfeldt, D. Janzén, S. F. Nunes, M. Antonsson, N. Van Zuydam, S. Skrtic, A. Hugerth, W. Weitschies, N. Davies, B. Abrahamsson, C.A.S. Bergström, In vitro and in vivo evaluation of 3D printed capsules with pressure triggered release mechanism for Oral peptide delivery, J. Pharm. Sci. 110 (2021) 228–238, https://doi.org/10.1016/j.xphs.2020.10.066.
[83] F.A. Dorkoosh, J.C. Verhoef, J.H.M. Verheijden, M. Rafiee-Tehrani, G. Borchard, H.E. Junginger, Peroral absorption of octreotide in pigs formulated in delivery systems on the basis of superporous hydrogel polymers, Pharm. Res. 19 (2002) 1532–1536, https://doi.org/10.1023/A:1020416918624.
[84] J. Wang, V. Yadav, A.L. Smart, S. Tajiri, A.W. Basit, Toward oral delivery of biopharmaceuticals: an assessment of the gastrointestinal stability of 17 peptide drugs, Mol. Pharm. 12 (2015) 966–973, https://doi.org/10.1021/mp500809f.
[85] A. Klepach, H. Tran, F. Ahmad Mohammed, M.E.H. ElSayed, Characterization and impact of peptide physicochemical properties on oral and subcutaneous delivery, Adv. Drug Deliv. Rev. 186 (2022) 114322, https://doi.org/10.1016/j.addr.2022.114322.
[86] F.A. Dorkoosh, J.C. Verhoef, G. Borchard, M. Rafiee-Tehrani, J.H.M. Verheijden, H.E. Junginger, Intestinal absorption of human insulin in pigs using delivery systems based on superporous hydrogel polymers, Int. J. Pharm. 247 (2002) 47–55, https://doi.org/10.1016/S0378-5173(02)00361-7.
[87] A.K. Dhalla, Z. Al-Shamsie, S. Beraki, A. Dasari, L.C. Fung, L. Fusaro, A. Garapaty, B. Gutierrez, D. Gratta, M. Hashim, K. Horlen, P. Karamchedu, R. Korupolu, E. Liang, C. Ong, Z. Owyang, V. Salgotra, S. Sharma, B. Syed, M. Syed, A.T. Vo, R. Abdul-Wahab, A. Wasi, A. Yamaguchi, S. Yen, M. Imran, A robotic pill for oral delivery of biotherapeutics: safety, tolerability, and performance in healthy subjects, Drug Deliv. Transl. Res. 12 (2022) 294–305, https://doi.org/10.1007/s13346-021-00938-1.
[88] Y.I.I.O. Yamagata, Sustained-Release Preparation Containing a Metal Salt of a Peptide, EP1002529A1, 2000.

[89] C. Yoshizane, A. Mizote, M. Yamada, N. Arai, S. Arai, K. Maruta, H. Mitsuzumi, T. Ariyasu, S. Ushio, S. Fukuda, Glycemic, insulinemic and incretin responses after oral trehalose ingestion in healthy subjects, Nutr. J. 16 (2017) 9, https://doi.org/10.1186/s12937-017-0233-x.

[90] H.A. Merchant, E.L. McConnell, F. Liu, C. Ramaswamy, R.P. Kulkarni, A.W. Basit, S. Murdan, Assessment of gastrointestinal pH, fluid and lymphoid tissue in the guinea pig, rabbit and pig, and implications for their use in drug development, Eur. J. Pharm. Sci. 42 (2011) 3–10, https://doi.org/10.1016/j.ejps.2010.09.019.

[91] G. Zheng, A.M. Torres, W.S. Price, WaterControl: self-diffusion based solvent signal suppression enhanced by selective inversion, Magn. Reson. Chem. 55 (2017) 447–451, https://doi.org/10.1002/mrc.4420.

[92] D. Sinnaeve, Simultaneous solvent and J-modulation suppression in PGSTE-based diffusion experiments, J. Magn. Reson. 245 (2014), https://doi.org/10.1016/j.jmr.2014.05.007.

[93] C. Dalvit, G.P. Fogliatto, A. Stewart, M. Veronesi, B. Stockman, WaterLOGSY as a method for primary NMR screening: practical aspects and range of applicability, J. Biomol. NMR 21 (2001) 349–359, https://doi.org/10.1023/A:1013302231549.

[94] E.L. McConnell, A.W. Basit, S. Murdan, Measurements of rat and mouse gastrointestinal pH, fluid and lymphoid tissue, and implications for in-vivo experiments, J. Pharm. Pharmacol. 60 (2010) 63–70, https://doi.org/10.1211/jpp.60.1.0008.

[95] I.R. Harris, H. Höppner, W. Siefken, K.-P. Wittern, A.M. Farrell, Regulation of HMG-CoA synthase and HMG-CoA reductase by insulin and epidermal growth factor in HaCaT keratinocytes, J. Invest. Dermatol. 114 (2000) 83–87, https://doi.org/10.1046/j.1523-1747.2000.00822.x.

[96] A.R. Garcia-Rendueles, J.S. Rodrigues, M.E.R. Garcia-Rendueles, M. Suarez-Fariña, S. Perez-Romero, F. Barreiro, I. Bernabeu, J. Rodriguez-Garcia, L. Fugazzola, T. Sakai, F. Liu, J. Cameselle-Teijeiro, S.B. Bravo, C.V. Alvarez, Rewiring of the apoptotic TGF-β-SMAD/NFκB pathway through an oncogenic function of p27 in human papillary thyroid cancer, Oncogene 36 (2017) 652–666, https://doi.org/10.1038/onc.2016.233.

[97] Z. Zeng, D. Qi, L. Yang, J. Liu, Y. Tang, H. Chen, X. Feng, Stimuli-responsive self-assembled dendrimers for oral protein delivery, J. Control. Release 315 (2019) 206–213, https://doi.org/10.1016/j.jconrel.2019.10.049.

[98] B. Chassaing, J.D. Aitken, M. Malleshappa, M. Vijay-Kumar, Dextran sulfate sodium (DSS)-induced colitis in mice, Curr. Protoc. Immunol. (2014), https://doi.org/10.1002/0471142735.im1525s104.

[99] I. Marigo, S. Zilio, G. Desantis, B. Mlecnik, A.H.R. Agnellini, S. Ugel, M.S. Sasso, J. E. Qualls, F. Kratochvill, P. Zanovello, B. Molon, C.H. Ries, V. Runza, S. Hoves, A. M. Bilocq, G. Bindea, E.M.C. Mazza, S. Bicciato, J. Galon, P.J. Murray, V. Bronte, T cell Cancer therapy requires CD40-CD40L activation of tumor necrosis factor and inducible nitric-oxide-synthase-producing dendritic cells, Cancer Cell 30 (2016) 377–390, https://doi.org/10.1016/j.ccell.2016.08.004.

[100] Z. Wei, E. Ting, Q.M. Yap, Z. Sun, J. Xing, Z. Zhan, A. Development, S. Centre, M. Sciences, Development of 2D-LC/MS/MS bioanalytical method for quantitative determination of insulin glargine in human plasma, ASMS MP 311 (2016) 1–7.